1

Linear polarization optimization for wideband MIMO systems with reconfigurable arrays

Miguel R. Castellanos, Member, IEEE and Robert W. Heath, Jr., Fellow, IEEE

Abstract-Reconfigurable arrays mold the propagation environment to benefit wireless systems. We use single-port polarization-reconfigurable antennas in a wideband multipleinput multiple-output (MIMO) system and demonstrate the efficacy of reconfiguration techniques based on analytical channel models. We apply a double-directional channel model to show that polarization reconfiguration acts as an additional precoding step on an unpolarized channel. We use Jensen's inequality to upper bound the spectral efficiency and leverage the relaxed objective to derive closed-form expressions for the optimal polarization angles at each antenna. We also derive upper bounds on the performance of a polarization reconfigurable system and develop an efficient procedure for polarization reconfiguration that aims to maximize these upper bounds. Numerical results show that the proposed simplified methods achieve near-optimal in wideband MIMO settings.

Index Terms—MIMO, polarization optimization, reconfigurable antenna, wideband communication.

I. INTRODUCTION

Reconfigurable antennas allow the system to change the composite wireless channel. Recent developments in reconfigurable antenna arrays have led to a wide variety in designs and capabilities [2]–[4]. Frequency and bandwidth tuning enable switching to different portions of the spectrum [5]. Gain pattern and polarization adaptation also enhances the array beamforming capabilities [6]. Reconfigurable antenna spacing and array orientation augment low-signal-to-noise-ratio (SNR) beamforming and high-SNR spatial multiplexing in sparse multipath channels [7] and line-of-sight channels [8]. By modifying the effective channel, including radio-frequency (RF), antenna, and propagation effects, reconfigurable systems increase the performance of wireless systems separately from other types of signal processing.

There are a large number of existing designs for reconfigurable antennas; the implementation significantly affects which parameters are modifiable and the extent of reconfigurability. Designs based on electronic switches, for example, use PIN diodes or RF microelectromechanical systems (MEMS) to shift between operating modes. These designs change frequency between two or more bands [9]–[11], switch

Our initial results were presented in Asilomar 2021, Pacific Grove, CA, USA [1]. This material is based upon work supported by the National Science Foundation under grants NSF-ECCS-2153698, NSF-CCF-2225555, NSF-CNS-2147955, in part by funds from federal agency and industry partners as specified in the Resilient & Intelligent NextG Systems (RINGS) program, and in part by Samsung and the affiliates of the NSF Broadband Wireless Access Center (BWAC) I/UCRC Center award NSF-CNS-1916766.

M. R. Castellanos, R. W. Heath are with the Department of Electrical and Computer Engineering, North Carolina State University, Raleigh, NC 27606 USA (e-mail: mrcastel@ncsu.edu; rwheathjr@ncsu.edu).

polarization angles [9], [12], alter the radiation pattern [9], [13], [14], and perform bandwidth reconfiguration [15]. While relatively easy to implement, switch-based antenna reconfiguration requires potentially bulky biasing circuitry and only provides a few modes of operation. Mechanical devices also provide tunable control of the electrical properties of antennas by moving different components [16], [17]. Mechanically reconfigurable antennas have the advantage of greater control and flexibility for reconfiguration over switches, but at the cost of increased complexity and power consumption. Novel materials, such as graphene metasurfaces and liquid metals, have also been used to create reconfigurable antennas that are more compact and operationally flexible. Metasurfaces have already been studied extensively for their use with antennas [18]–[20] and antenna arrays [21]–[25], altering the characteristics of antennas to achieve a wideband operation and increased gain with a low-profile. Room temperature liquid metals also enable a great degree of reconfigurability by leveraging a large range of conductor arrangements [26]–[29]. The aforementioned solutions enable the reconfigurability of numerous antenna parameters at various frequency bands and can therefore be readily implemented in existing wireless deployments.

Reconfigurable arrays increase the throughput of MIMO systems by promoting beneficial channel conditions. For example, reconfigurable systems combat depolarization, improve array directivity and beamforming, and switch operating frequencies to improve signal reception. The use of reconfigurable gain patterns has been applied to a variety of problems in wireless communication, including single-user MIMO [30], [31], multi-user MIMO [32], multi-hop communication [33], and channel estimation and mode selection [34]. Joint polarization reconfiguration at the transmitter and receiver increases throughput by adapting to the channel depolarization conditions [35], [36]. Other array properties, such as the array spacing and orientation improve performance by adjusting the rank and singular values of the channel depending on the SNR [7], [8]. An important benefit of reconfigurable antennas is that the aforementioned functions can be leveraged concurrently with advanced signal processing algorithms.

We focus on the use of a single-port polarization reconfigurable arrays to increase the performance in a wideband single-user MIMO system. While efficient in terms of size constraints, dual-polarized systems require double the number of RF chains since each array element has two ports. This can lead to increased power consumption and more complex feeding, especially in systems with a large number of antennas [36], [37]. The reduced power consumption of

polarization reconfigurable arrays could be leveraged for lowenergy devices or to enable higher quality RF components, such as high-resolution data converters. In addition, some types of reconfigurable antennas, such as metasurface antennas [25], [38], function as large contiguous apertures. This can significantly impact their implementation as co-located dualpolarized arrays. While there is a substantial body of work focusing on dual-polarized arrays [39]–[45], there are only a few studies that have leveraged single-port polarization reconfiguration. The achievable rate benefits of polarization reconfigurable antennas are studied from a signal processing perspective in [35], [36], where a norm objective is used to develop an iterative approach to polarization optimization in a narrowband setting. Polarization reconfiguration and spatial modulation are combined in [46] to develop an efficient resource allocation algorithm. An experimental setup in [47] consisting of two quad-polarized antennas demonstrates that polarization diversity increases the system achievable rate by leveraging uncorrelated polarization channels. Results in [48] also show how channel depolarization knowledge can be used to perform power allocation across two orthogonal polarizations to achieve significant SNR gains.

We solve the problem of optimizing the linear polarization of each antenna in a polarization reconfigurable wideband MIMO system to maximize the spectral efficiency. Compared to our preliminary work [1], which only addresses polarization reconfiguration at the transmitter in a narrowband communication, we provide a more thorough analysis of polarization reconfiguration and provide new methods for polarization reconfiguration at both the transmitter and receiver. We use the double-directional channel model in [49] to account for the effects of channel and antenna depolarization, relative rotations, and the co-polarization and cross-polarization of each antenna element. Rather than directly optimizing the spectral efficiency, we relax the optimization objective by using Jensen's inequality to maximize the sum of the channel Frobenius norm for each subcarrier. The relaxed objective and the analytical channel model allows us to derive closedform expressions for the polarization of one of the arrays when the polarization of the other array is fixed. Polarization reconfiguration at both ends can then be achieved in an iterative fashion. In contrast to prior work on polarization reconfiguration [35], [36], [46]–[48], we provide closed-form expressions for the optimized polarization angles and objective function in a more general wideband scenario, which simplifies the joint polarization optimization. In addition, these expressions are leveraged in analyzing the system performance in the remainder of the work. This analysis raises a number of key insights related to how the channel relates to the optimal polarization angle.

To simplify the optimization, we also suggest a subarray approach to polarization reconfiguration. Subarray architectures are useful in MIMO systems with limited numbers of RF chains due to lower hardware complexity with only a small loss in performance [50], [51]. Likewise, the subarray method simplifies the hardware design in a reconfigurable system by allowing the polarization of groups of antennas to be controlled in conjunction. For example, metasurface

antennas which are tuned using biasing voltages can all be controlled simultaneously. In addition, a mechanically reconfigurable array that is rotated to change the polarization of all the antennas together can also use this method. We also derive upper bounds on the sum channel norm based on the unpolarized channel matrix, which is defined later, and develop a method for polarization reconfiguration based on maximizing those bounds. Simulation results with wideband systems demonstrate the efficacy of both the subarray approach and the bound maximization method, which indicates that polarization reconfiguration can be successfully achieved with low feedback and computational overhead.

This paper is organized as follows: In Section II, we describe the signal model, reconfigurable array model, and the channel model. In Section III, we formulate the polarization optimization problem and derive methods for optimization. In Section IV, we derive the channel norm upper bounds and discuss a method for polarization reconfiguration based on maximizing those bounds. We discuss the overhead associated with quantized polarization reconfiguration feedback in Section V. In Section VI, we present numerical results to showcase the proposed methods. We summarize the results and provide concluding remarks in Section VII.

Notation: A bold lowercase letter a denotes a column vector, a bold uppercase letter A denotes a matrix. The matrix A^{\perp} denotes the transpose of A, A^{\dagger} denotes the nontransposed conjugate of A, A* denotes the conjugate transpose of A, and $\|A\|_F$ denotes the Frobenius norm of A. $\mathbf{D} = \operatorname{diag}(d_1, d_2, \dots, d_N)$ denotes the diagonal matrix D with diagonal entries given by d_1, d_2, \dots, d_N and $\mathbf{B} = \text{blkdiag}(\mathbf{D}_1, \mathbf{D}_2, \dots, \mathbf{D}_N)$ denotes the block diagonal matrix B composed of the blocks $\mathbf{D}_1, \mathbf{D}_2, \dots, \mathbf{D}_N$ along the diagonal. For an $N \times N$ Hermitian matrix \mathbf{A} , $\lambda_n(\mathbf{A})$ denotes the *n*th dominant eigenvalue ordered in descending fashion with $\lambda_1(\mathbf{A})$ being the largest. The distribution $\mathcal{N}(\mu, \sigma^2)$ denotes a circularly-symmetric complex Gaussian with mean μ and variance σ^2 . We denote $j = \sqrt{-1}$. For a complex number z = x + jy, we denote Re[z] = x and Im[z] = y. The function $\tan_2^{-1}(a, b)$ denotes the two-argument inverse tangent, which finds the angle between the positive xaxis and the line to the point connecting the origin and the point (a,b), and $1_{\mathcal{A}}(\cdot)$ denotes the indicator function of the set A. The operator \odot denotes the element-wise product for matrices and the operator \otimes denotes the Kronecker product for matrices.

II. SYSTEM MODEL

In this section, we describe the models for the different components of the system. We overview the wideband MIMO signal model. We then describe the model for a polarization reconfigurable array. We incorporate the array model into a double-directional channel model that accounts for both antenna and channel depolarization. We conclude the section by developing an equivalent model that separates the reconfigurable component from the rest of the channel.

A. Signal model

We first present the signal model of a single-user wideband MIMO system using ortogonal frequency-division multiplex-

ing (OFDM). A transmitter equipped with $N_{\rm t}$ antennas communicates with a receiver equipped with $N_{\rm r}$ antennas. The transmitter sends $N_{\rm s}$ data streams across K subcarriers to the receiver. The symbol vector for the kth subcarrier $\mathbf{s}_k \in \mathbb{C}^{N_{\rm s}}$ is precoded with $\mathbf{F}_k \in \mathbb{C}^{N_{\rm t} \times N_{\rm s}}$ yielding the transmit signal

$$\mathbf{x}_k = \mathbf{F}_k \mathbf{s}_k. \tag{1}$$

We assume the symbol vector is zero-mean and satisfies $\mathbb{E}\left[\mathbf{s}_{k}\mathbf{s}_{k}^{*}\right]=\mathbf{I}_{N_{s}}.$

The transmit signal is sent across the frequency-selective channel $\mathbf{H}_k \in \mathbb{C}^{N_{\mathrm{r}} \times N_{\mathrm{t}}}$. The receive antennas observe the signal \mathbf{y}_k . We assume perfect synchronization at the receiver. Both time and frequency synchronization are not affected by the polarization reconfigurable antennas and can be performed using standard methods in literature [52]. Let \mathbf{n}_k denote the noise vector for the kth subcarrier with independent and identically distributed entries with distribution $\mathcal{N}(0, \sigma_{\mathrm{n}}^2)$. The received signal is then given by

$$\mathbf{y}_k = \mathbf{H}_k \mathbf{F}_k \mathbf{s}_k + \mathbf{n}_k. \tag{2}$$

To simplify the analysis of polarization reconfiguration, we assume an optimum receiver that can jointly decode the received data streams [53].

While this appears to be a standard MIMO signal model, the addition of reconfigurable antennas plays an important role in the channel model. We now discuss the reconfigurable antenna array models. We also discuss antenna polarization and its effect on the array characteristics.

B. Array model

Electromagnetic waves radiated by antennas are composed of oscillating electric and magnetic fields that are perpendicular to the direction of propagation. The polarization of an antenna generally refers to the orientation of the electric field oscillations. Antennas are commonly designed with an intended polarization, which is referred to as the copolarization. A component of the radiated field may also be present in the orthogonal polarization, referred to as the cross-polarization. Let ϕ be direction-of-departure or -arrival, which accounts for both the azimuthal angle ϕ_{az} and the elevation angle ϕ_{el} . For a given antenna, let $\mathcal{G}_{C}(\phi)$ denote the gain pattern in the co-polarization direction and $\mathcal{G}_{X}(\phi)$ denote the gain pattern in the cross-polarization direction. The cross-pol pattern is generally much weaker than the co-pol pattern in linear polarized systems, but elliptical and circular polarization require the two polarization patterns to have nearequal strength. As an example, we can denote the inverse cross-polarization discrimination (XPD) of an antenna as χ_{ant} and let $\mathcal{G}_{C} = 1/\sqrt{1+\chi_{\mathsf{ant}}}$ and $\mathcal{G}_{\mathsf{X}} = \sqrt{\chi_{\mathsf{ant}}/1+\chi_{\mathsf{ant}}}$ for all angles. Antennas generally exhibit high XPDs, meaning that χ_{ant} is small. The net antenna gain pattern is characterized by examining the gain pattern in two orthogonal polarization directions.

The antenna gain pattern can also be expressed in terms of horizontal direction and vertical directions, which are specified with reference to the antenna coordinate system, i.e., locally. Let $\mathcal{G}_H(\phi)$ be the horizontal polarization gain

pattern and $\mathcal{G}_V(\phi)$ be the vertical polarization gain pattern. The relationship between the co-pol/cross-pol patterns and the horizontal/vertical patterns are captured through a simple coordinate rotation. Let θ denote the antenna co-polarization angle and define $\mathbf{Q}(\theta)$ to be the Givens rotation matrix

$$\mathbf{Q}(\theta) = \begin{bmatrix} \cos \theta & \sin \theta \\ -\sin \theta & \cos \theta \end{bmatrix}. \tag{3}$$

Then, we have the following expression relating the two sets of coordinates:

$$\left[\mathcal{G}_{\mathsf{H}}(\phi) \ \mathcal{G}_{\mathsf{V}}(\phi)\right]^{\mathsf{T}} = \mathbf{Q}(\theta) \left[\mathcal{G}_{\mathsf{C}}(\phi) \ \mathcal{G}_{\mathsf{X}}(\phi)\right]^{\mathsf{T}}.\tag{4}$$

The local co-pol and cross-pol coordinates will be used for describing the antenna patterns of the transmitter and receiver, while the horizontal and vertical coordinates will provide a common reference to characterize propagation over the wireless channel.

Array responses can be described using a vector $\mathbf{a}(\phi)$ that specifies the relative phase differences between the antenna elements. For an N element uniform linear array operating at wavelength λ and inter-element spacing d, the array response vector at azimuth angle ϕ_{az} is

$$\mathbf{a}(\phi_{\mathsf{az}}) = \left[1 \ e^{-\mathrm{j}2\pi\frac{d}{\lambda}\sin\phi_{\mathsf{az}}} \cdots e^{-\mathrm{j}2\pi\frac{d}{\lambda}(N-1)\sin\phi_{\mathsf{az}}}\right]^{\mathsf{T}}.$$
 (5)

For a uniform planar array, the array response vector needs to account for the azimuth angle $\phi_{\rm az}$ and elevation angle $\phi_{\rm el}$. If the array is in the yz-plane with N_y elements in the y-direction and N_z elements in the N_z direction, the two-dimensional array response can be vectorized as

$$\mathbf{a}(\phi_{\mathsf{az}}, \phi_{\mathsf{el}}) = \begin{bmatrix} 1 & \cdots & e^{-\mathrm{j}2\pi\frac{d}{\lambda}(n_y\sin\phi_{\mathsf{az}}\sin\phi_{\mathsf{el}} + n_z\cos\phi_{\mathsf{el}}) & \cdots \\ e^{-\mathrm{j}2\pi\frac{d}{\lambda}((N_y - 1)\sin\phi_{\mathsf{az}}\sin\phi_{\mathsf{el}} + (N_z - 1)\cos\phi_{\mathsf{el}}) \end{bmatrix}^\mathsf{T}.$$
(6

Here, we assume the vectorization is applied over the y-axis, but it can also be applied over the z-axis. The array response vector in this form, however, only provides a mean of analyzing the response of an array of isotropic antennas. In practice, the antenna responses, which include the gain patterns and polarizations, should also be taken into account.

We apply the array model in [49] to model the array response of an array of non-isotropic antennas. Since the antenna gain patterns are separated into two polarization components, we define the $N \times 2$ array response matrix $\mathbf{A}(\phi)$ to account for the phase, gain pattern, and polarization differences. For the nth antenna, let $\mathcal{G}_{\mathsf{H},n}$ denote the horizontal gain pattern and $\mathcal{G}_{\mathsf{V},n}$ denote the vertical gain pattern. We define the array net response matrix as

$$\mathbf{A}_{\mathsf{net}}(\phi) = \left(\mathbf{a}(\phi) \otimes \begin{bmatrix} 1 \end{bmatrix}\right) \odot \begin{bmatrix} \mathcal{G}_{\mathsf{H},1}(\phi) & \mathcal{G}_{\mathsf{V},1}(\phi) \\ \vdots & \vdots \\ \mathcal{G}_{\mathsf{H},N}(\phi) & \mathcal{G}_{\mathsf{V},N}(\phi) \end{bmatrix}. \tag{7}$$

The array net response matrix is composed of two columns, each of which corresponds to a modified array response vector that accounts for the gain pattern of a particular polarization.

The array net response matrix in (7) expressed in terms of the co-polarization gain $\mathcal{G}_{\mathsf{C},n}$ and cross-polarization gain $\mathcal{G}_{\mathsf{X},n}$. We let $\theta_{\mathsf{C},n}$ denote the polarization angle of the nth antenna and let $\boldsymbol{\theta} = [\theta_1 \dots \theta_N]$ be a vector containing the polarization angles for the entire array. We additionally define the polarization angle vector for an angle $\boldsymbol{\theta}$ as

$$\mathbf{p}(\theta) = \left[\cos\theta \sin\theta\right]^{\mathsf{T}},\tag{8}$$

the polarization matrix for the array as

$$\mathbf{P}(\boldsymbol{\theta}) = \text{blkdiag}(\mathbf{p}(\theta_1), \dots, \mathbf{p}(\theta_N))$$
 (9)

and the antenna gain matrix $\mathbf{J}_n(\boldsymbol{\phi})$ as

$$\mathbf{J}_{n}(\phi) = \begin{bmatrix} \mathcal{G}_{\mathsf{C},n}(\phi) & \mathcal{G}_{\mathsf{X},n}(\phi) \\ \mathcal{G}_{\mathsf{X},n}(\phi) & -\mathcal{G}_{\mathsf{C},n}(\phi) \end{bmatrix}. \tag{10}$$

Then, the array net response matrix is then expressed as

$$\mathbf{A}_{\mathsf{net}}(\boldsymbol{\phi}) = \left\{ \mathbf{a}(\boldsymbol{\phi}) \otimes [1 \ 1] \right\} \odot \mathbf{P}^{\mathsf{T}}(\boldsymbol{\theta}) \left[\begin{array}{c} \mathbf{J}_{1}(\boldsymbol{\phi}) \\ \vdots \\ \mathbf{J}_{N}(\boldsymbol{\phi}) \end{array} \right]. \quad (11)$$

In this form, the effect of polarization $A_{net}(\phi)$ is completely specified by $P(\theta)$.

We assume that both the receive and transmit arrays are polarization reconfigurable. We model reconfigurability of the array as the ability to control θ within a feasible set Θ . When each polarization angle θ_n changes, the antenna effectively rotates its polarization relative to the horizontal and vertical directions. Unless otherwise stated, each antenna is assumed to be able to individually reconfigure its polarization. This models a polarization change in a *linearly* polarized system. While changes from linear to and from circular or elliptical polarization could also be modeled, this requires the co-pol and cross-pol gain patterns to change as well. For analytical tractability, we will assume that the gain patterns of each antenna do not change as a function of the polarization angle.

The feasible set of polarizations depends on the degree of reconfigurability of the system. For the majority of this paper, we will assume that each polarization angle θ lies in the range $[-\pi/2, \pi/2)$. The coordinate change relationship (4) shows that a polarization angle rotation of π results in a phase shift of π of both patterns. Since this phase term is arbitrary, we restrict the feasible set of polarizations to have a range of π without loss of generality. A practical scenario in which the polarizations are quantized is discussed in Section V.

C. Channel model

The wideband channel model is obtained by combining the array model with a double-directional channel model as in [49]. The channel is composed of L paths from the transmitter to the receiver. The ℓ th path is distinguished by a complex path gain α_{ℓ} , a path delay τ_{ℓ} , a direction of departure (DOD) $\phi_{\ell,t}$, a direction of arrival (DOA) $\phi_{\ell,r}$ and a 2×2 depolarization matrix \mathbf{X}_{ℓ} . In addition, we denote ψ as the rotation angle between the local polarization coordinates at the transmitter and the local polarization coordinates at the receiver. We let $v(\tau)$ be the filter that captures low-pass filtering and pulse

shaping as a function of time τ , and let T denote the sampling period.

We first describe the time-domain and frequency-domain representations of the channel. In the remainder of the paper, we will use the subscripts t to denote transmit-side and r to denote receive-side. For a channel with D delay taps, the discrete delay d channel \mathbf{H}_d is given by

$$\mathbf{H}_{d} = \sum_{\ell=1}^{L} \alpha_{\ell} v(dT - \tau_{\ell}) \mathbf{A}_{\mathsf{net},\mathsf{r}}(\boldsymbol{\phi}_{\ell,\mathsf{r}}) \mathbf{Q}(\psi) \mathbf{X}_{\ell,d} \left(\mathbf{A}_{\mathsf{net},\mathsf{t}}(\boldsymbol{\phi}_{\ell,\mathsf{t}}) \right)^{\mathsf{T}},$$
(12)

where the depolarization matrix varies over lag. Let the coefficient $v_{\ell,k}$ denote

$$\mathsf{v}_{\ell,k} = \sum_{d=0}^{D-1} v(dT - \tau_{\ell}) e^{\frac{-j2\pi kd}{K}},\tag{13}$$

and let $\mathbf{X}_{\ell,k}$ be the 2×2 depolarization matrix for the kth subcarrier and ℓ th path. We also combine the terms α_{ℓ} and $\mathbf{v}_{\ell,k}$ into a single term $\beta_{\ell,k}$. Then the channel frequency response matrix for the kth subcarrier is given as

$$\mathbf{H}_{k} = \sum_{\ell=1}^{L} \beta_{\ell,k} \mathbf{A}_{\mathsf{net},\mathsf{r}}(\boldsymbol{\phi}_{\ell,\mathsf{r}}) \mathbf{Q}(\psi) \mathbf{X}_{\ell,k} \left(\mathbf{A}_{\mathsf{net},\mathsf{t}}(\boldsymbol{\phi}_{\ell,\mathsf{t}}) \right)^{\mathsf{T}}. \quad (14)$$

While not explicitly stated, the array steering matrices can also vary as a function of the subcarrier k, for example, in cases where beam squint is relevant. We focus on frequency-domain processing in the remainder of this paper.

We leverage an alternate channel representation to simplify the polarization reconfiguration operation. For convenience, we momentarily assume a single-path channel and drop the path index ℓ . Let H_{k,n_r,n_t} denote the (n_r,n_t) th element of \mathbf{H}_k , a_{r,n_r} be the n_r th element of the receive steering vector, and a_{t,n_t} be the n_t th element of the transmit steering vector. Expanding (14) and using the fact that

$$\mathbf{Q}(\theta) \begin{bmatrix} \mathcal{G}_{\mathsf{C}}(\phi) & \mathcal{G}_{\mathsf{X}}(\phi) \end{bmatrix}^{\mathsf{T}} = \mathbf{J}(\phi)\mathbf{p}(\theta), \tag{15}$$

the elements of the channel are

$$\mathsf{H}_{k,n_{\mathsf{r}},n_{\mathsf{t}}} = \mathbf{p}^{\mathsf{T}}(\theta_{\mathsf{r},n_{\mathsf{r}}})\mathbf{J}_{\mathsf{r},n_{\mathsf{r}}}\left(\beta_{k} \, a_{\mathsf{r},n_{\mathsf{r}}}(\boldsymbol{\phi}_{\mathsf{r}})\mathbf{Q}(\psi)\mathbf{X}_{k} a_{\mathsf{t},n_{\mathsf{t}}}(\boldsymbol{\phi}_{\mathsf{t}})\right) \times \mathbf{J}_{\mathsf{t},n_{\mathsf{t}}}^{\mathsf{T}}\mathbf{p}(\theta_{\mathsf{t},n_{\mathsf{t}}}). \tag{16}$$

The polarization vectors, as defined in (8), effectively combine the two orthogonal polarizations present in the channel at the transmitter and receiver. We then define the *unpolarized* channel for antenna pair (n_r, n_t) as the 2×2 matrix

$$\mathbf{H}_{\mathsf{up},k,n_{\mathsf{r}},n_{\mathsf{t}}} = \mathbf{J}_{\mathsf{r},n_{\mathsf{r}}} \left(\beta_k \, a_{\mathsf{r},n_{\mathsf{r}}}(\boldsymbol{\phi}_{\mathsf{r}}) \mathbf{Q}(\boldsymbol{\psi}) \mathbf{X}_k a_{\mathsf{t},n_{\mathsf{t}}}^\mathsf{T}(\boldsymbol{\phi}_{\mathsf{t}}) \right) \mathbf{J}_{\mathsf{t},n_{\mathsf{t}}}^\mathsf{T}.$$
(17)

The term "unpolarized" here refers to the fact that the polarizations of the arrays are not included. To construct the unpolarized channel matrix for all of the antennas, we let $\overline{\mathbf{J}}_{\ell}$ denote the $2N \times 2N$ block diagonal matrix

$$\overline{\mathbf{J}}_{\ell} = \text{blkdiag}\left(\mathbf{J}_{1}(\boldsymbol{\phi}_{\ell}), \dots, \mathbf{J}_{N}(\boldsymbol{\phi}_{\ell})\right).$$
 (18)

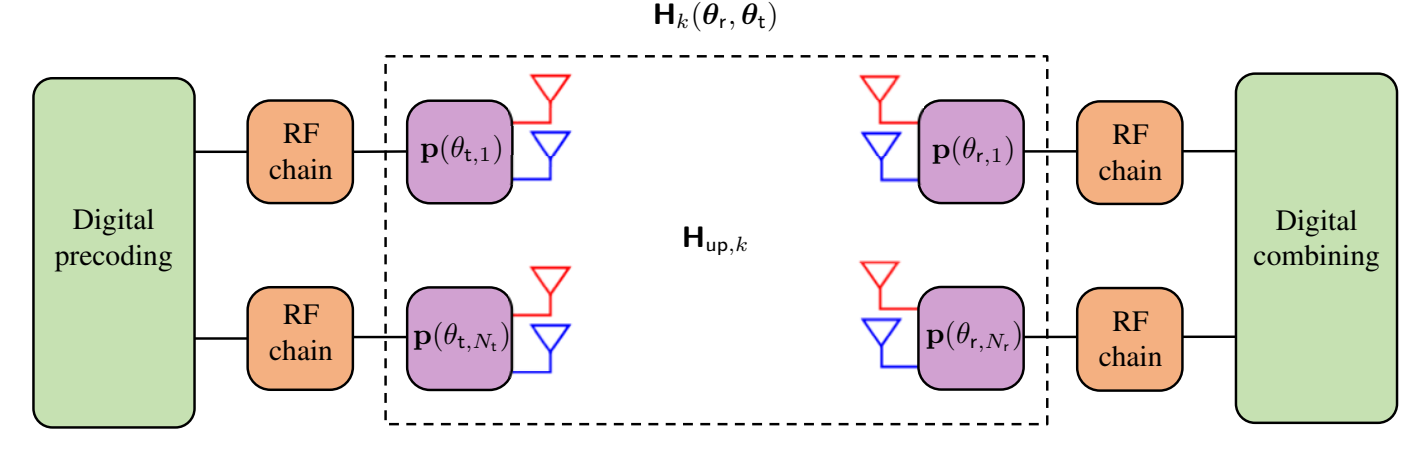


Fig. 1: Illustration of the polarization reconfigurable MIMO system. The channel $\mathbf{H}_k(\boldsymbol{\theta}_r, \boldsymbol{\theta}_t)$ is represented by polarization precoding and combining over the unpolarized channel $\mathbf{H}_{up,k}$.

Reintroducing the multi-path channel and the subcarrier index k, the unpolarized MIMO channel is then be expressed as

$$\mathbf{H}_{\mathsf{up},k} = \sum_{\ell=1}^{L} \overline{\mathbf{J}}_{\mathsf{r},\ell}^{\mathsf{T}} \left(\left(\beta_{\ell,k} \mathbf{a}_{\mathsf{r}}(\boldsymbol{\phi}_{\ell,\mathsf{r}}) \mathbf{a}_{\mathsf{t}}^{\mathsf{T}}(\boldsymbol{\phi}_{\ell,\mathsf{t}}) \right) \otimes \mathbf{Q}(\psi) \mathbf{X}_{\ell,k} \right) \overline{\mathbf{J}}_{\mathsf{t},\ell}.$$
(19)

The unpolarized MIMO channel effectively acts as a virtual dual-polarized channel, where each array element is composed of two orthogonally polarized antennas. Unlike a dual-polarized system, however, the reconfigurable system only has a single port for each antenna.

The polarized channel \mathbf{H}_k is computed by reincorporating the polarization of each antenna. Let θ_r be the receive polarization angle vector and θ_t be the transmit polarization angle vector. Then the channel matrix is given by

$$\mathbf{H}_{k}(\boldsymbol{\theta}_{r}, \boldsymbol{\theta}_{t}) = \mathbf{P}^{\mathsf{T}}(\boldsymbol{\theta}_{r}) \mathbf{H}_{\mathsf{up}, k} \mathbf{P}(\boldsymbol{\theta}_{t}). \tag{20}$$

The polarization matrices effectively combine the entries of the unpolarized channel according to the polarization of each antenna at the transmitter and receiver, as shown in Fig. 1.

The benefit of the decomposition shown in (20) is that it decouples the polarization reconfiguration from the rest of the channel. In this manner, the unpolarized channel $\mathbf{H}_{up,k}$ does not change when reconfiguring the arrays, and the matrices \mathbf{P} is designed based on $\mathbf{H}_{up,k}$. In the next section, we leverage this channel representation to optimize the polarization angle at the transmitter and the receiver.

D. Problem formulation

We now formulate the polarization angle optimization for the wideband MIMO system. Both the transmit and receive arrays are assumed to be polarization reconfigurable. As discussed in Section II-B, we model reconfigurability by assuming that θ_t and θ_r are adjustable. This changes the polarization matrices, which then affects the channel matrix.

We assume that both \mathbf{H}_k and $\mathbf{H}_{up,k}$ are known at the transmitter and receiver. The unpolarized channel can be estimated by training with two orthogonal polarizations at each end, where each polarized channel can be obtained using existing

channel estimation algorithms from the literature. From (16), by appropriately setting both $\theta_{\rm r,n_r}=0,\pi/2$ and $\theta_{\rm t,n_t}=0,\pi/2$, the entries of each 2×2 matrix in (17), are isolated. Other orthogonal polarization pairs could also be applied in tandem with an appropriate linear transformation to obtain $\mathbf{H}_{\rm up,k}$.

The system objective is to find the polarization angle vectors θ_t and θ_r and precoder **F** to maximize the mutual information given a transmit power constraint P. This optimization is formulated as

$$\max_{\boldsymbol{\theta}_{t} \in \Theta_{t}, \, \boldsymbol{\theta}_{r} \in \Theta_{r}, \mathbf{F}} \sum_{k=1}^{K} \log_{2} \left| \mathbf{I} + \frac{1}{\sigma_{n}^{2}} \mathbf{H}_{k}(\boldsymbol{\theta}_{r}, \boldsymbol{\theta}_{t}) \mathbf{F}_{k} \mathbf{F}_{k}^{*} \mathbf{H}_{k}^{*}(\boldsymbol{\theta}_{r}, \boldsymbol{\theta}_{t}) \right|$$

$$s.t. \sum_{k=1}^{K} \operatorname{tr}(\mathbf{F}_{k}^{H} \mathbf{F}_{k}) \leq P.$$
(21)

For fixed transmit and receive polarizations, an appropriate choice of precoder \mathbf{F}_k diagonalizes the channel, and the optimal achievable rate is obtained by waterfilling over the channel [53]. Waterfilling diagonalizes the channel and then allocates power $P_{s,k}$ to the sth stream and kth subcarrier. The resulting achievable spectral efficiency is given by

$$C\left(\left\{\mathbf{H}_{k}(\boldsymbol{\theta}_{r}, \boldsymbol{\theta}_{t})\right\}_{k=1}^{K}\right)$$

$$= \sum_{k=1}^{K} \sum_{s=1}^{N_{s}} \log_{2}\left(1 + \frac{\lambda_{s}(\mathbf{H}_{k}(\boldsymbol{\theta}_{r}, \boldsymbol{\theta}_{t})\mathbf{H}_{k}^{*}(\boldsymbol{\theta}_{r}, \boldsymbol{\theta}_{t}))P_{s,k}}{\sigma_{n}^{2}}\right).$$
(22)

Given the water level μ , the powers $p_{s,k}$ is calculated as

$$P_{s,k} = \left(\mu - \frac{\sigma^2}{\lambda_s(\mathbf{H}_k(\boldsymbol{\theta}_r, \boldsymbol{\theta}_t)\mathbf{H}_k^*(\boldsymbol{\theta}_r, \boldsymbol{\theta}_t))}\right), \qquad (23)$$

and μ is then chosen to satisfy the total power constraint

$$\sum_{k=1}^{K} \sum_{s=1}^{s} P_{s,k} = P. \tag{24}$$

Unfortunately, the intertwined nature of the polarization angles and waterfilling solution make it difficult to directly optimize (22).

We apply Jensen's inequality to (22) to separate the effect of polarization reconfiguration from precoding. Exploiting log det concavity [53],

$$C\left(\left\{\mathbf{H}_{k}(\boldsymbol{\theta}_{\mathsf{r}}, \boldsymbol{\theta}_{\mathsf{t}})\right\}_{k=1}^{K}\right) \leq KN_{\mathsf{s}} \log_{2}\left(1 + \frac{1}{KN_{\mathsf{s}}} \sum_{k=1}^{K} \sum_{s=1}^{N_{\mathsf{s}}} \frac{\lambda_{s}(\mathbf{H}_{k}(\boldsymbol{\theta}_{\mathsf{r}}, \boldsymbol{\theta}_{\mathsf{t}})\mathbf{H}_{k}^{*}(\boldsymbol{\theta}_{\mathsf{r}}, \boldsymbol{\theta}_{\mathsf{t}}))P_{s,k}}{\sigma_{\mathsf{n}}^{2}}\right) \leq KN_{\mathsf{s}} \log_{2}\left(1 + \frac{P}{KN_{\mathsf{s}}\sigma_{\mathsf{n}}^{2}} \sum_{k=1}^{K} \left\|\mathbf{H}_{k}(\boldsymbol{\theta}_{r}, \boldsymbol{\theta}_{t})\right\|_{F}^{2}\right), \tag{25}$$

where the first inequality follows from Jensen's inequality and the second from the total power constraint. A uniform power allocation would result in equality in the second step. The bound in (25) only depends on the polarization angle vectors at the transmitter and receiver. We therefore focus on optimizing the polarization angles by maximizing the upper bound as

$$\max_{\boldsymbol{\theta}_{\mathsf{t}} \in \Theta_{\mathsf{t}}, \, \boldsymbol{\theta}_{\mathsf{r}} \in \Theta_{\mathsf{r}}} \quad \sum_{k=1}^{K} \left\| \mathbf{P}_{\mathsf{r}}^{\mathsf{T}} \mathbf{H}_{\mathsf{up}, k} \mathbf{P}_{\mathsf{t}} \right\|_{F}^{2}. \tag{26}$$

Once the optimal polarization angles are found, the precoder is then designed to waterfill over the reconfigured channel. While the power constraint does not play a part in (26), it will affect the spectral efficiency performance once waterfilling is performed over the optimized channel. We also note that the analysis could also be extended to hybrid and analog precoding by designing the precoder to approximate the optimal waterfilling solution over $\mathbf{H}(\theta_r, \theta_t)$. As shown in the following sections, the relaxation yields feasible optimizations of the polarization angles.

III. WIDEBAND MIMO POLARIZATION ANGLE OPTIMIZATION

We develop a few different solutions to the problem in (26) in this section. We present a method that is optimal but requires a difficult multivariate optimization, as well as a suboptimal but efficient algorithm based on an upper bound maximization. We describe how to optimize the transmit and receive polarization angles separately. We discuss the case in which the polarization angle of each antenna is reconfigured separately, and a subarray approach in which groups of antennas have the same polarization. We end the section with a discussion on joint optimization of the transmit and receive polarizations.

A. Unilateral polarization optimization

For this first method the system aims to maximize $\sum_{k=1}^{K} \left\| \mathbf{P}^{\mathsf{T}}(\boldsymbol{\theta}_{\mathsf{r}}) \mathbf{H}_{\mathsf{up},k} \mathbf{P}(\boldsymbol{\theta}_{\mathsf{t}}) \right\|_{F}^{2}$ by optimizing one of the polarization matrices given the other is fixed. For simplicity, we will drop the dependence of the polarization matrix $\mathbf{P}(\boldsymbol{\theta}_{\mathsf{C}}^{\mathsf{t}})$ on $\boldsymbol{\theta}_{\mathsf{C}}^{\mathsf{t}}$ and simply denote it as \mathbf{P}_{t} . Similarly, we will let $\mathbf{P}_{\mathsf{r}} = \mathbf{P}(\boldsymbol{\theta}_{\mathsf{C}}^{\mathsf{r}})$.

We show that unilateral polarization optimization of each antenna can be performed independently from the other elements. In the case that \mathbf{P}_r is fixed, we define the matrix \mathbf{C}_r as

$$\mathbf{C}_{\mathsf{r}} = \sum_{k=1}^{K} \mathbf{H}_{\mathsf{up},k}^{*} \mathbf{P}_{\mathsf{r}} \mathbf{P}_{\mathsf{r}}^{\mathsf{T}} \mathbf{H}_{\mathsf{up},k}, \tag{27}$$

which we will refer to as the receive-polarized channel Gram matrix. Similarly, if \mathbf{P}_t is fixed, we define the transmit-polarized channel Gram matrix as

$$\mathbf{C}_{\mathsf{t}} = \sum_{k=1}^{K} \mathbf{H}_{\mathsf{up},k} \mathbf{P}_{\mathsf{t}} \mathbf{P}_{\mathsf{t}}^{\mathsf{T}} \mathbf{H}_{\mathsf{up},k}^{*}. \tag{28}$$

The objective function in (26) is then expressed as

$$\sum_{k=1}^{K} \left\| \mathbf{P}_{r}^{\mathsf{T}} \mathbf{H}_{\mathsf{up},k} \mathbf{P}_{t} \right\|_{F}^{2} = \operatorname{tr} \left(\mathbf{P}_{t}^{T} \mathbf{C}_{r} \mathbf{P}_{t} \right) = \operatorname{tr} \left(\mathbf{P}_{r}^{T} \mathbf{C}_{t} \mathbf{P}_{r} \right). \tag{29}$$

Without loss of generality, the system focuses optimizing the length N angle vector $\boldsymbol{\theta}$ for the $2N \times 2N$ unilaterally polarized channel Gram matrix \mathbf{C} as

$$\theta_{\text{opt}} = \operatorname*{argmax}_{\boldsymbol{\theta} \in \Theta} \operatorname{tr} \left(\mathbf{P}^{\mathsf{T}}(\boldsymbol{\theta}) \mathbf{C} \mathbf{P}(\boldsymbol{\theta}) \right).$$
 (30)

To simplify (30), we partition C into 2×2 block matrices and denote the (i,j)th block matrix as $C_{i,j}$. Due to the block diagonal form of P, the nth diagonal term of the matrix P^TCP , denoted as γ_n and referred to as the nth postpolarization gain, is written in terms of the polarization vectors $\mathbf{p}_n = \mathbf{p}(\theta_n)$ as

$$\gamma_n = \mathbf{p}_n^\mathsf{T} \mathbf{C}_{n,n} \mathbf{p}_n. \tag{31}$$

The nth polarization can be optimized by maximizing the corresponding post-polarization gain.

The following Lemma describes how to find the optimal polarization angle given $C_{n,n}$.

Lemma 1. Let \mathbf{C} be a 2×2 Hermitian matrix with (i, j)th entry $c_{i,j}$, and let $\mathbf{p}(\theta) = [\cos \theta \sin \theta]^\mathsf{T}$. Then, the angle θ that maximizes $\mathbf{p}^\mathsf{T}(\theta)\mathbf{C}\mathbf{p}(\theta)$ is given as

$$\theta_{\mathsf{opt}}(\mathbf{C}) = \underset{\theta}{\operatorname{argmax}} \mathbf{p}^{\mathsf{T}}(\theta) \mathbf{C} \mathbf{p}(\theta)$$
$$= -\frac{1}{2} \tan_{2}^{-1} (2 \operatorname{Re}[c_{1,2}], c_{1,1} - c_{2,2}). \tag{32}$$

The optimal value is given as

$$\max_{\theta} \mathbf{p}^{\mathsf{T}}(\theta) \mathbf{C} \mathbf{p}(\theta) = \lambda_1(\text{Re}[\mathbf{C}])$$

$$= \frac{c_{1,1} + c_{2,2}}{2} + \sqrt{\left(\frac{c_{1,1} - c_{2,2}}{2}\right)^2 + \text{Re}\left[c_{1,2}\right]^2}.$$
(33)

Proof: The objective $\mathbf{p}(\theta)\mathbf{C}\mathbf{p}(\theta)$ is written as

$$\mathbf{p}^{\mathsf{T}}(\theta)\mathbf{C}\mathbf{p}(\theta)$$

$$= \begin{bmatrix} \mathbf{p}^{\mathsf{T}}(\theta) & 0 & 0 \end{bmatrix} \begin{bmatrix} \operatorname{Re}[\mathbf{C}] & -\operatorname{Im}[\mathbf{C}] \\ \operatorname{Im}[\mathbf{C}] & \operatorname{Re}[\mathbf{C}] \end{bmatrix} \begin{bmatrix} \mathbf{p}(\theta) & 0 & 0 \end{bmatrix}^{\mathsf{T}}$$

$$= \mathbf{p}^{\mathsf{T}}(\theta)\operatorname{Re}[\mathbf{C}]\mathbf{p}(\theta). \tag{34}$$

Since Re[C] is a real symmetric 2×2 matrix, it admits a decomposition in terms of a rotation matrix with angle φ and a diagonal matrix $\mathbf{\Lambda} = \text{diag}(\lambda_a, \lambda_b)$ as [54]

$$Re[\mathbf{C}] = \mathbf{Q}^{\mathsf{T}}(\varphi) \mathbf{\Lambda} \mathbf{Q}(\varphi).$$
 (35)

The vector \mathbf{x} that maximizes $\mathbf{x}^T \operatorname{Re}[\mathbf{C}]\mathbf{x}$ is one of the eigenvectors of $\operatorname{Re}[\mathbf{C}]$, which is either $\mathbf{p}(-\varphi)$ or $\mathbf{p}(-\varphi + \pi/2)$ depending on the ordering of λ_a and λ_b . From [54], $\lambda_a \geq \lambda_b$

when $c_{1,1} \ge c_{2,2}$, and $\lambda_a < \lambda_b$ otherwise. The optimal angle, denoted as $\theta_{opt}(\mathbf{C})$ is therefore given as

$$\theta_{\text{opt}}(\mathbf{C}) = -\varphi \pm 1_{[\lambda_1, \infty)}(\lambda_2) \cdot \pi/2,$$
 (36)

where the \pm is irrelevant due to the invariance of the objective to sign changes of the solution vector but included for simplification purposes. Using [54, eq. (3.5)], the optimal angle is written in terms of the elements of \mathbf{C} as in (32), where the \pm allows the simplification to \tan_2^{-1} . The optimal value in (33) is given by the largest eigenvalue of $\operatorname{Re}[\mathbf{C}]$, which is obtained in closed-form from [54, eqs. (3.2)-(3.3)].

Lemma 1 is applied to each of the $\mathbf{C}_{n,n}$ to obtain the nth optimal angle that maximizes the post-polarization gain, given as $\theta_{\mathsf{opt}}(\mathbf{C}_{n,n})$. Letting $\boldsymbol{\theta}_{\mathsf{opt}}(\mathbf{C}) = [\theta_{\mathsf{opt}}(\mathbf{C}_{1,1}) \cdots \theta_{\mathsf{opt}}(\mathbf{C}_{N,N})]^\mathsf{T}$, Lemma 1 also yields the optimal value of the objective in (30) as

$$\operatorname{tr}\left(\mathbf{P}^{\mathsf{T}}(\boldsymbol{\theta}_{\mathsf{opt}}(\mathbf{C}))\mathbf{C}\mathbf{P}(\boldsymbol{\theta}_{\mathsf{opt}}(\mathbf{C}))\right) = \sum_{n=1}^{N} \lambda_{1}(\operatorname{Re}[\mathbf{C}_{n,n}]).$$
 (37)

The optimal angles and values can be computed efficiently using fast diagonalization techniques [54] or the cosine-sine decomposition [55].

Remark 1: The optimal angle expression given in (32) lies in the range $[-\pi/2, \pi/2)$. This corresponds with the intuition that rotating the polarization angle by π will not affect the system.

Remark 2: Lemma 1 highlights the relationship between the optimal polarization angle and the eigendecomposition of the real part of the unilaterally polarized channel Gram matrix C. Only the real part of C is relevant for the optimization because the system optimizes over linear polarizations, in which the co-pol and cross-pol components are in-phase. We expect that a polarization reconfiguration method that allowed elliptical polarizations would involve the imaginary part of C as well.

As noted earlier, the unilateral reconfiguration method can be applied to find both the transmit polarization and receive polarization with the proper definition of C. This method can be applied when only one side of the link is reconfigurable. An alternating maximization using this maximization to iteratively optimize the receive and transmit polarizations could also be applied as discussed in [36]. As an alternative, we develop a solution that is guaranteed to maximize the channel norm and a practical solution that is easy to compute. The closed-form expression for the optimal polarization will allow us to develop and analyze the performance of different reconfiguration techniques in the following sections.

B. Subarray optimization

The method presented in the previous section finds the optimal polarization for each antenna assuming individual reconfiguration. We show that the system can perform a similar technique when groups of antennas use the same polarization angle by simply grouping the post-polarization gains and appropriately applying Lemma 1. We will also demonstrate that this subarray method is suboptimal to the array optimization and discuss cases in which equality holds.

We again drop the notation indicating whether we are targeting the receiver or the transmitter. Let $\mathcal{N}=\{1,2,\ldots,N\}$ denote the indices of the antenna elements. Let M denote the number of subarrays and let $\mathcal{N}_m\subseteq\mathcal{N}$ denote the mth subarray. We assume that the set of subarrays $\mathcal{P}=\{\mathcal{N}_m\}_{m=1}^M$ is mutually exclusive and collectively exhaustive, i.e., $\bigcup_{m=1}^M \mathcal{N}_m=\mathcal{N}$ and $\mathcal{N}_{m_1}\cap\mathcal{N}_{m_2}=\emptyset$ for $m_1\neq m_2$. The subarray polarization constraint restricts the polarization angle of each antenna in subarray \mathcal{N}_m to be equal so that $\theta_{n_1}=\theta_{n_2}$ for any $n_1,\ n_2\in\mathcal{N}_m$.

From (31), if the polarization angles of each antenna in a subarray are identical, then the corresponding $\mathbf{C}_{n,n}$ can be added together to find the optimal polarization for the subarray. We define the subarray unilaterally polarized channel Gram matrix as

$$\mathbf{C}_{\mathcal{N}_m} = \sum_{n \in \mathcal{N}_m} \mathbf{C}_{n,n}.$$
 (38)

The optimal polarization angle for subarray \mathcal{N}_m is then obtained by applying Lemma 1 and taking $\mathbf{C}_{\mathcal{N}_m}$ as the argument, yielding the angle $\theta_{\text{opt}}(\mathbf{C}_{\mathcal{N}_m})$. We let $\theta_{\text{opt},\mathcal{P}}(\mathbf{C})$ denote the optimal polarization angle vector for the subarray partition \mathcal{P} . The nth entry of $\theta_{\text{opt},\mathcal{P}}(\mathbf{C})$ is given by $\sum_{m=1}^M \theta_{\text{opt}}(\mathbf{C}_{\mathcal{N}_m}) 1_{\mathcal{N}_m}(n)$ and the resulting channel norm is given by

$$\operatorname{tr}\left(\mathbf{P}^{\mathsf{T}}(\boldsymbol{\theta}_{\mathsf{opt},\mathcal{P}}(\mathbf{C}))\mathbf{C}\mathbf{P}(\boldsymbol{\theta}_{\mathsf{opt},\mathcal{P}}(\mathbf{C}))\right) = \sum_{m=1}^{M} \lambda_{1}(\operatorname{Re}[\mathbf{C}_{\mathcal{N}_{m}}]).$$
(39)

The per-element and subarray reconfiguration methods are directly compared, and the following result shows the sub-optimality of the subarray approach.

Lemma 2. Let $\mathcal{P}_1 = \{\mathcal{N}_m^{(1)}\}_{m=1}^{M_1}$ and $\mathcal{P}_2 = \{\mathcal{N}_m^{(2)}\}_{m=2}^{M_2}$ be two subarray partitions with N divisible by both. Let k be a positive integer and $M_1 = kM_2$. Furthermore, assume that the subarray partition \mathcal{P}_2 subdivides \mathcal{P}_1 , i.e.,

$$\mathcal{N}_{m}^{(1)} = \bigcup_{j=k(m-1)+1}^{km} \mathcal{N}_{j}^{(2)}.$$
 (40)

Then, the optimized channel norm of the coarser partition is smaller than that of the finer one:

$$\operatorname{tr}\left(\mathbf{P}^{\mathsf{T}}(\boldsymbol{\theta}_{\mathsf{opt},\mathcal{P}_{1}}(\mathbf{C}))\mathbf{C}\mathbf{P}(\boldsymbol{\theta}_{\mathsf{opt},\mathcal{P}_{1}}(\mathbf{C}))\right)$$

$$\leq \operatorname{tr}\left(\mathbf{P}^{\mathsf{T}}(\boldsymbol{\theta}_{\mathsf{opt},\mathcal{P}_{2}}(\mathbf{C}))\mathbf{C}\mathbf{P}(\boldsymbol{\theta}_{\mathsf{opt},\mathcal{P}_{2}}(\mathbf{C}))\right).$$
(41)

If, furthermore, we have that for each $m=1,...,M_1$, $\operatorname{Re}[\mathbf{C}_{\mathcal{N}_m^{(1)}}]$ and $\operatorname{Re}[\mathbf{C}_{\mathcal{N}_{k(m-1)+1}^{(2)}}],\cdots,[\mathbf{C}_{\mathcal{N}_{km}^{(2)}}]$ have the same dominant eigenvector, then equality holds in (41).

Proof: From (39), it suffices to show that $\sum_{m=1}^{M_1} \lambda_1([\mathbf{C}_{\mathcal{N}_m^{(1)}}]) \leq \sum_{m=1}^{M_2} \lambda_1([\mathbf{C}_{\mathcal{N}_m^{(2)}}])$. Applying Weyl's inequality for eigenvalues of sums of Hermitian matrices

[56], we have

$$\sum_{m=1}^{M_1} \lambda_1(\operatorname{Re}[\mathbf{C}_{\mathcal{N}_m^{(1)}}])$$

$$= \sum_{m=1}^{M_1} \lambda_1 \left(\sum_{j=k(m-1)+1}^{km} \operatorname{Re}[\mathbf{C}_{\mathcal{N}_j^{(2)}}] \right)$$

$$\leq \sum_{m=1}^{M_1} \sum_{j=k(m-1)+1}^{km} \lambda_1(\operatorname{Re}[\mathbf{C}_{\mathcal{N}_j^{(2)}}])$$

$$= \sum_{m=1}^{M_2} \lambda_1(\operatorname{Re}[\mathbf{C}_{\mathcal{N}_m^{(2)}}]). \tag{42}$$

The equality condition is verified from the definition of an eigenvector. Let \mathbf{v}_m be the dominant eigenvector of $\mathrm{Re}[\mathbf{C}_{\mathcal{N}_m^{(1)}}]$ and $\mathrm{Re}[\mathbf{C}_{\mathcal{N}_{k(m-1)+1}^{(2)}}],\cdots,[\mathbf{C}_{\mathcal{N}_{km}^{(2)}}]$. It follows that for each m

$$\lambda_{1} \left(\operatorname{Re}[\mathbf{C}_{\mathcal{N}_{m}^{(1)}}] \right) = \operatorname{Re}[\mathbf{C}_{\mathcal{N}_{m}^{(1)}}] \mathbf{v}_{m}$$

$$= \sum_{j=k(m-1)+1}^{km} \operatorname{Re}[\mathbf{C}_{\mathcal{N}_{j}^{(2)}}] \mathbf{v}_{m}$$

$$= \sum_{j=k(m-1)+1}^{km} \lambda_{1} \left(\operatorname{Re}[\mathbf{C}_{\mathcal{N}_{j}^{(2)}}] \right). \tag{43}$$

Therefore, equality holds in (42).

Remark 3: This theorem demonstrates that allowing more antennas to be reconfigurable will increase the resulting channel norm. At the two extremes, we see that per-element reconfigurability will lead to the highest norm, and reconfiguring the array as a whole will result in the lowest norm. We show equality holds in Lemma 2 for single-path propagation when the antennas in each array have the same gain patterns. We will examine transmit polarization reconfiguration and take $C = C_r$. For this case, we assume that all transmit antennas have the same gain pattern and assume likewise with the receive antennas. We further assume that each receive antenna is identically polarized with angle θ_r in this example. We define the matrix $\mathbf{R}(\theta)$ as

$$\mathbf{R}(\theta) = \begin{bmatrix} \cos^2 \theta & \cos \theta \sin \theta \\ \cos \theta \sin \theta & \sin^2 \theta \end{bmatrix}. \tag{44}$$

Then,

$$\mathbf{C}_{\mathsf{r},n,n} = N_{\mathsf{r}} |\beta|^2 |\omega_k|^2 \mathbf{J}_{\mathsf{t}}^* \mathbf{X}^* \mathbf{Q}(\psi)^{\mathsf{T}} \mathbf{J}_{\mathsf{r}}^{\dagger} \mathbf{R}(\theta_{\mathsf{r}}) \mathbf{J}_{\mathsf{r}}^{\mathsf{T}} \mathbf{Q}(\psi) \mathbf{X} \mathbf{J}_{\mathsf{t}}.$$
(45)

Each $C_{r,n,n}$ is not dependent on n and, therefore, all share the same eigenvectors. From the conditions in Lemma 2, the optimal polarization reconfiguration at each transmit antenna achieves the same channel norm as optimal polarization reconfiguration of the array as a whole. This result is intuitive since the receive antennas are identically polarized and the transmit antenna polarizations only need to be matched for the single path.

C. Joint polarization optimization

So far, we have derived the optimal polarization angle at one transceiver to maximize the channel norm given the polarization at the other end is fixed. We now leverage the derived expressions to find the optimal polarization angle at the other end of the link.

For clarity, we describe the algorithm from the perspective of the receiver, but the procedure can be applied at the transmitter as well. The optimal polarization angle at the transmitter is computed in terms of the matrix \mathbf{C}_t defined in (28). This matrix can be expressed in terms of the polarization angle at the receiver and the unpolarized channel matrix $\mathbf{H}_{up,k}$. Using the definition of the unpolarized channel entries in (17), \mathbf{C}_{r,n_t,n_t} is expressed as

$$\mathbf{C}_{\mathsf{r},n_{\mathsf{t}},n_{\mathsf{t}}} = \sum_{k=1}^{K} \sum_{n_{\mathsf{r}}=1}^{N_{\mathsf{r}}} (\mathbf{H}_{\mathsf{up},k,n_{\mathsf{r}},n_{\mathsf{t}}})^* \mathbf{R}(\theta_{\mathsf{r},n_{\mathsf{r}}}) \mathbf{H}_{\mathsf{up},k,n_{\mathsf{r}},n_{\mathsf{t}}}. \tag{46}$$

Recalling (33), the optimal channel norm after unilateral reconfiguration is determined by the elements of \mathbf{C}_{r,n_t,n_t} . Because of this, the optimized channel norm can be written in terms of the polarization angles $\theta_{r,m}$. Closed-form expressions for the channel norm in terms of $\theta_{r,m}$ can be obtained by expanding the matrix product in (46) but are omitted due to space limitations.

For joint optimization, the system, therefore, first solves the problem

$$\boldsymbol{\theta}_{r, \mathsf{opt}} = \underset{\boldsymbol{\theta}_r \in \Theta_r}{\operatorname{argmax}} \ \operatorname{tr} \left(\mathbf{P}^\mathsf{T}(\boldsymbol{\theta}_{\mathsf{opt}}(\mathbf{C}_r(\boldsymbol{\theta}_r))) \mathbf{C}_r \mathbf{P}(\boldsymbol{\theta}_{\mathsf{opt}}(\mathbf{C}_r(\boldsymbol{\theta}_r))) \right), \tag{47}$$

where the dependence of C_r on θ_r is explicitly stated. Once the optimal receive polarization is found, the system computes C_r and the optimal transmit polarization angle $\theta_{t,opt}(C_r)$. The dimensionality of the optimization can be significantly reduced through subarray method. In this case, the system sets the appropriate constraints on the receive polarization angle and solves the joint optimization as before. Let $\mathcal{P}_r\{\mathcal{N}_{r,m}\}_{m=1}^{M_r}$ be the set of receive subarrays with M_r elements and $\mathcal{P}_t\{\mathcal{N}_{t,m}\}_{m=1}^{M_t}$ the set of transmit subarrays with M_t elements. The systems first finds the optimal receive polarization angle with the appropriate subarray constraint as

$$\theta_{\mathsf{r},\mathsf{opt}}$$

$$= \underset{\theta_{\mathsf{r}} \in \Theta_{\mathsf{r}}}{\operatorname{argmax}} \operatorname{tr} \left(\mathbf{P}^{\mathsf{T}} (\theta_{\mathsf{opt},\mathcal{P}_{\mathsf{t}}} (\mathbf{C}_{\mathsf{r}}(\theta_{\mathsf{r}}))) \mathbf{C}_{\mathsf{r}} \mathbf{P} (\theta_{\mathsf{opt},\mathcal{P}_{\mathsf{t}}} (\mathbf{C}_{\mathsf{r}}(\theta_{\mathsf{r}}))) \right)$$

$$s.t. \ \theta_{\mathsf{r},i} = \theta_{\mathsf{r},j} \ \text{if} \ i, j \in \mathcal{N}_{\mathsf{r},m}, \ \forall m = 1, 2, \dots, M_{\mathsf{r}}.$$

The optimal transmit polarization is then given as $\theta_{t,opt} = \theta_{opt,\mathcal{P}_t}(\mathbf{C}_r(\theta_{r,opt}))$. The transmit subarray constraint is also included in the objective function. In Section VI, we show that the subarray method achieves performance close to that of per-element reconfiguration.

IV. PERFORMANCE BOUNDS

In this section, we derive upper bounds on the sum channel Frobenius norm. We leverage the bounds to derive a lowcomplexity method for joint optimization of the transmit and receive polarization angles. The key result of this section is given in the Lemma 3, which gives an upper bound for unilateral reconfiguration in terms of C_r or C_t . An upper bound for joint reconfiguration is also given in Lemma 4.

Lemma 3. Let θ_r be a fixed polarization angle vector at the receiver. For any transmit polarization angle vector θ_t , we have the following upper bound:

$$\sum_{k=1}^{K} \left\| \mathbf{H}_{k}(\boldsymbol{\theta}_{\mathsf{r}}, \boldsymbol{\theta}_{\mathsf{t}}) \right\|_{F}^{2} \leq \operatorname{tr}(\mathbf{C}_{\mathsf{r}}). \tag{49}$$

Likewise, if θ_t *is fixed, then*

$$\sum_{k=1}^{K} \left\| \mathbf{H}_{k}(\boldsymbol{\theta}_{\mathsf{r}}, \boldsymbol{\theta}_{\mathsf{t}}) \right\|_{F}^{2} \leq \operatorname{tr}(\mathbf{C}_{\mathsf{t}})$$
 (50)

for any θ_r .

Proof: From (29), we have that

$$\sum_{k=1}^{K} \left\| \mathbf{P}_{r}^{\mathsf{T}} \mathbf{H}_{\mathsf{up}, k} \mathbf{P}_{t} \right\|_{F}^{2} = \operatorname{tr} \left(\mathbf{P}_{t}^{\mathsf{T}} \mathbf{C}_{r} \mathbf{P}_{t} \right). \tag{51}$$

We will use the Poincaré Separation Theorem [57, p. 190] to bound (51). Let \mathbf{A} be an arbitrary $M \times M$ Hermitian matrix, and let \mathbf{B} be a $M \times N$ semi-unitary matrix such that $N \leq M$ and $\mathbf{B}^*\mathbf{B} = \mathbf{I}$. The Poincaré Separation Theorem states that

$$\lambda_{i+M-N}(\mathbf{A}) \le \lambda_i(\mathbf{B}^H \mathbf{A} \mathbf{B}) \le \lambda_i(\mathbf{A}).$$
 (52)

Applying (52) to (29) with $A = C_r$ and $B = P_t$, we have

$$\operatorname{tr}\left(\mathbf{P}_{t}^{T}\mathbf{C}_{r}\mathbf{P}_{t}\right) = \sum_{n_{t}=1}^{2N_{t}} \lambda_{n_{t}}(\mathbf{P}_{t}^{\mathsf{T}}\mathbf{C}_{r}\mathbf{P}_{t})$$

$$\leq \sum_{n_{t}=1}^{N_{t}} \lambda_{n_{t}}(\mathbf{C}_{r})$$

$$= \operatorname{tr}(\mathbf{C}_{r}), \tag{53}$$

where we have used the fact that C_r is rank N_t . Similar steps are applied to obtain (50).

Lemma 4. For any polarization angle vectors θ_r and θ_t , the following inequality holds:

$$\sum_{k=1}^{K} \|\mathbf{H}_{k}(\boldsymbol{\theta}_{r}, \boldsymbol{\theta}_{t})\|_{F}^{2} \leq \sum_{k=1}^{K} \|\mathbf{H}_{\mathsf{up}, k}\|_{F}^{2}.$$
 (54)

Proof: We start with the inequality in the previous theorem

$$\sum_{k=1}^{K} \left\| \mathbf{H}_{k}(\boldsymbol{\theta}_{\mathsf{r}}, \boldsymbol{\theta}_{\mathsf{t}}) \right\|_{F}^{2} \leq \operatorname{tr}(\mathbf{C}_{\mathsf{r}}) = \sum_{k=1}^{K} \operatorname{tr}(\mathbf{P}_{\mathsf{r}}^{\mathsf{T}} \mathbf{H}_{\mathsf{up}, k} \mathbf{H}_{\mathsf{up}, k}^{*} \mathbf{P}_{\mathsf{r}}).$$
(55)

We again apply the Poincaré Separation Theorem to (55) to obtain

$$\begin{split} \sum_{k=1}^{K} \operatorname{tr} \left(\mathbf{P}_{\mathsf{r}}^{\mathsf{T}} \mathbf{H}_{\mathsf{up},k} \mathbf{H}_{\mathsf{up},k}^{*} \mathbf{P}_{\mathsf{r}} \right) &\leq \sum_{k=1}^{K} \sum_{n_{\mathsf{r}}=1}^{N_{\mathsf{r}}} \lambda_{n_{\mathsf{r}}} \left(\mathbf{H}_{\mathsf{up},k} \mathbf{H}_{\mathsf{up},k}^{*} \right) \\ &= \sum_{k=1}^{K} \operatorname{tr} \left(\mathbf{H}_{\mathsf{up},k} \mathbf{H}_{\mathsf{up},k}^{*} \right) \\ &= \sum_{k=1}^{K} \left\| \mathbf{H}_{\mathsf{up},k} \right\|_{F}^{2}, \end{split}$$

which completes the proof.

Remark 4: The inequalities in Lemmas 3 and 4 are tighter than what would be obtained by applying the bound $\|\mathbf{AB}\|_F^2 \leq \|\mathbf{A}\|_F^2 \|\mathbf{B}\|_F^2$. For example, applying this bound would result in

$$\left\| \mathbf{H}(\boldsymbol{\theta}_{\mathsf{r}}, \boldsymbol{\theta}_{\mathsf{t}}) \right\|_{F}^{2} \leq N_{\mathsf{r}} N_{\mathsf{t}} \left\| \mathbf{H}_{\mathsf{up}, k} \right\|_{F}^{2}, \tag{56}$$

which is larger than the proposed bound and becomes worse as we scale the number of antennas.

In Lemma 3, we have essentially bounded the sum channel Frobenius norm in terms of the unpolarized channel $\mathbf{H}_{\text{up},k}$ and the polarization angle at the receiver or transmitter. Rather than performing the joint optimization by solving (47), the system optimize the upper bound in Lemma 3 and then use this angle to find the polarization at the other end. We again describe the algorithm from the perspective of the receiver and attempt to maximize the upper bound $\operatorname{tr}(\mathbf{C}_r)$. We have that $\operatorname{tr}(\mathbf{C}_r) = \operatorname{tr}(\mathbf{P}_r^\mathsf{T}(\sum_{k=1}^K \mathbf{H}_{\text{up},k}\mathbf{H}_{\text{up},k})\mathbf{P}_r)$. Therefore, the system applies the same algorithm as in Section III-A to find the receive polarization angle that maximizes this upper bound. We denote this approach as the bound maximization (BM) approach.

We let $\theta_{r,BM}$ denote the receive polarization vector that maximizes $tr(\mathbf{C}_r)$, given as

$$\boldsymbol{\theta}_{\mathsf{r},\mathsf{BM}} = \operatorname*{argmax}_{\boldsymbol{\theta}_{\mathsf{r}} \in \Theta_{\mathsf{r}}} \mathrm{tr}(\mathbf{C}_{\mathsf{r}}) = \boldsymbol{\theta}_{\mathsf{opt}} \left(\sum_{k=1}^{K} \mathbf{H}_{\mathsf{up},k}^{*} \mathbf{H}_{\mathsf{up},k} \right).$$
 (57)

The system uses this angle to compute $\mathbf{P}(\theta_{r,BM})$ and get the optimized matrix \mathbf{C}_r , denoted as $\mathbf{C}_{r,BM}$. The system then computes the transmit polarization angle vector as

$$\theta_{\text{t.BM}} = \theta_{\text{opt}}(\mathbf{C}_{\text{r.BM}}).$$
 (58)

As in the previous cases, this method can be combined with the subarray method at either or both of the arrays.

The BM approach does not require the system to solve a complicated optimization, as both $\theta_{r,BM}$ and $\theta_{t,BM}$ is computed using the closed-form expressions in Section III-A. As shown in the numerical results, the BM approach achieves performance close to that of the joint polarization optimization and is therefore a viable method for a practical polarization reconfiguration.

V. FEEDBACK CONSIDERATIONS

Feedback of the optimal polarization angles enables polarization reconfiguration at the transmitter in scenarios in which only the receiver has knowledge of the unpolarized channel. In these cases, it may be practical to quantize the polarization angles prior to transmission to reduce overhead. In addition, the subarray method discussed in Section III-B reduces overhead by decreasing the number of angles in the feedback.

Quantization of the polarization angle can be restricted to the range $[-\pi/2,\pi/2)$ due to the periodicity of the effect of polarization on the channel. Let $b_{\rm q}$ denote the number of bits used to quantize the polarization angle. Then the polarization angle θ are quantized as $\theta_{\rm q}$ from the quantization set $\Omega_{\rm q}$ as follows:

$$\theta_{\mathsf{q}} = \underset{\vec{\theta} \in \Omega_{\mathsf{q}}}{\operatorname{argmin}} \left| (\theta - \vec{\theta}) \operatorname{mod} \pi \right|, \tag{59}$$

where

$$\Omega_{\mathsf{q}} = \left\{ -\frac{\pi}{2}, \, \frac{\pi}{2^{b_{\mathsf{q}}}} - \frac{\pi}{2}, \, \cdots, \, \frac{(2^{b_{\mathsf{q}}} - 1)\pi}{2^{b_{\mathsf{q}}}} - \frac{\pi}{2} \right\}. \tag{60}$$

By quantizing the polarization angles to $[-\pi/2, \pi/2)$ instead of $[0, 2\pi)$ (as discussed in [36]) we double the quantization resolution for a given number of bits.

Due to the iterative nature of the optimization methods we have discussed, quantization can be performed pre-transmit-optimization or post-transmit-optimization. In pre-transmit-optimization quantization, the receiver quantizes the optimal receive polarization angles, transmit these to the transmitter, and let the transmitter optimize its own polarization based on the feedback. In post-transmit-optimization, the receiver optimizes both the transmit and receive polarizations, and then feeds forward the quantized transmit polarization angles to the receiver. We focus on post-transmit-optimization quantization, since the alternative requires having at least partial knowledge of the unpolarized channel matrix. While pre-transmit-optimization quantization may be preferable in certain cases due to computational complexity, we focus on post-transmit-optimization quantization as it is more practically relevant.

The overhead required to feed back the quantized polarization angles depends on the number of quantization bits and the number of subarrays used for polarization reconfiguration. The number of feedback overhead bits b_f are computed as

$$b_{\mathsf{f}} = b_{\mathsf{g}} + \lceil \log_2(M_{\mathsf{t}}) \rceil. \tag{61}$$

In a time-division duplexing system, the same polarization angles can be used for both uplink and downlink. To inform the transmitter of the precoder, the receiver either feeds back the channel state information after applying the calculated transmit and receive polarization or a quantized precoder. We leave the precoder quantization and feedback overhead as a topic for future work. In the following section, we show simulation results for different quantization and subarray resolutions and compare the corresponding feedback overheads.

VI. NUMERICAL RESULTS

In this section, we provide some simulation results showcase the performance of the proposed polarization reconfiguration methods. We obtain results with channels generated using the multi-ray geometric model described in Section II. We also use the QuaDRiGa channel simulator to demonstrate the efficacy of the polarization reconfigurable system using measurement-based channels with more sophisticated path and depolarization models.

A. Results with double-directional channel model

In this section, we use the double-directional channel model described in Section II to generate the MIMO channel. We assume that both the DOAs and DODs have azimuth angles uniformly distributed in $[-\pi,\pi)$ and elevation angles uniformly distributed in $[-\pi/2,\pi/2)$. The antenna arrays are modeled as UPAs with half-wavelength spacing at both the transmitter and receiver. Unless otherwise stated, all antenna gain patterns are assumed to be identical. The rotation angle ψ is also uniformly distributed in the range $[-\pi,\pi)$. In all methods, we perform waterfilling over the number of subcarriers and $N_{\rm s}=4$ streams.

Channel depolarization changes the phase and amplitude of the two signal polarization components, effectively changing the polarization of the signal. To model channel depolarization, we define χ as the inverse XPD and α_ℓ^{AB} as the phase change induced when going from polarization A to polarization B. We then use a frequency-flat correlation model in which

$$\mathbf{X}_{\ell} = \sqrt{\frac{1}{1+\chi}} \begin{bmatrix} e^{j\alpha_{\ell}^{\mathsf{HH}}} & \sqrt{\chi}e^{j\alpha_{\ell}^{\mathsf{HV}}} \\ \sqrt{\chi}e^{j\alpha_{\ell}^{\mathsf{VH}}} & e^{j\alpha_{\ell}^{\mathsf{VV}}} \end{bmatrix}. \tag{62}$$

Unless otherwise stated, the parameter χ will be set to 0.2 as in [45].

We also simulate antenna depolarization by including a small amount of energy leakage from the co-polarization to the cross-polarization. Each antenna is modeled identically, and we assume that the antenna gain pattern does not change as a function of the direction of arrival or departure. We let the inverse XPD for the antenna be defined as $\chi_{\rm ant}$, let $\mathcal{G}_{\rm C}=1/\sqrt{1+\chi_{\rm ant}}$ and $\mathcal{G}_{\rm X}=\sqrt{\chi_{\rm ant}/1+\chi_{\rm ant}}$. With these definitions, we ensure $|\mathcal{G}_{\rm C}|^2+|\mathcal{G}_{\rm X}|^2=1$. In all simulations, we set $\chi_{\rm ant}=0.1$.

In Fig.2 we plot the spectral efficiency of different polarization reconfiguration methods compared to the transmit SNR, which is defined as SNR = P/σ_n^2 . We simulate a wideband 4×4 MIMO system. We model a channel with L=2 paths as in [58]. The number of subcarriers is set to K = 64 and the number of channel taps is D=16. The pulse-shaping filter is assumed to be a raised-cosine pulse with rolloff factor 0.3. Since reconfiguration changes the norm of the channel, we normalize the unpolarized channel as $\sum_{k=1}^{K} \mathbb{E}[\|\mathbf{H}_{\text{up},k}\|_F^2] = 4KN_rN_t$ to ensure a fair comparison. As baselines, we employ static methods in which the respective array retains its polarization. In this setting, we simulate a static array as having all of the antennas horizontally polarized. If both array polarizations are optimized, then the solution is obtained from the joint polarization optimization in Section III-C. The brute force approach works by searching over possible polarization angles to directly maximize the achievable rate expression in (22). The proposed method in Sec. III-C optimizes the sum channel norm, while the brute force search maximizes the achievable rate.

The results demonstrate that any level of polarization reconfiguration noticeably increases the system performance, while

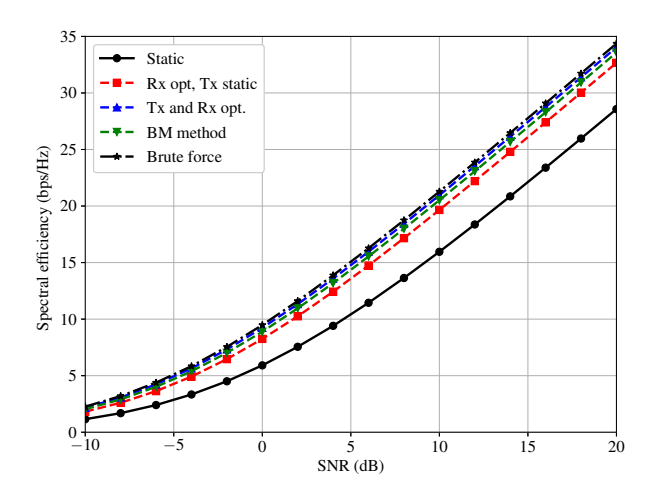


Fig. 2: Spectral efficiency vs. SNR for different polarization reconfiguration methods in a wideband 4×4 MIMO system. Frequency-flat polarization reconfiguration achieves gains over the static method even in a wideband setting.

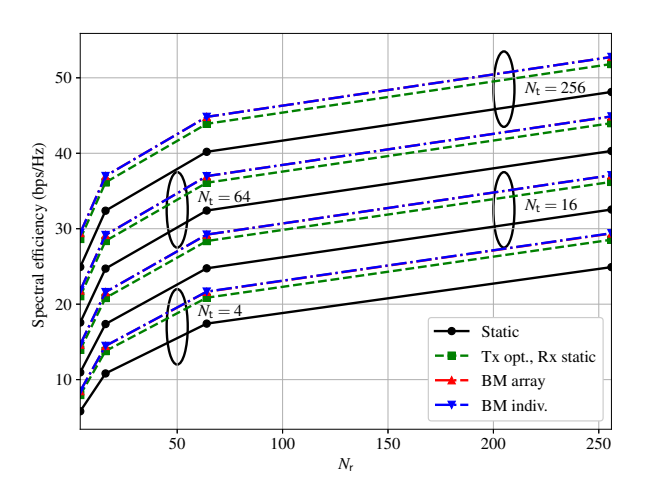


Fig. 3: Spectral efficiency for different MIMO sizes. We simulate $N_{\rm r}=4,16,64,256$ and $N_{\rm t}=4,16,64,256$. Optimization at both ends of the link becomes more important for larger array sizes.

reconfiguration at both ends of the link achieves the highest performance. Both the BM method and the joint optimization method perform close to the brute force optimization. Even though polarization reconfiguration is frequency-flat, it achieves a gain over the static method.

The effect of the number of antennas on the system on the polarization reconfiguration methods is shown in Fig. 3. We use the same parameters for the wideband setting as in the previous simulation, but the number of channel paths is set to L=2 and the SNR is fixed as 0 dB. We compare the performance of polarization optimization at one end compared to the BM method. For the BM method, we examine two cases in which the entire array is forced to

have the same polarization and another in which each antenna has individual polarization control. Even though the subarray method only reconfigures a single parameter, it achieves very close to the individual reconfiguration technique. Polarization reconfiguration at both ends becomes more relevant as the size of the arrays increases.

B. Results with QuaDRiGa

In this section, we present simulation results using the realistic channel simulator QuaDRiGa [59]. The simulator generates cluster-based double-directional channels by randomly generating channel parameters using distributions obtained from measurement campaigns. Arbitrary antenna patterns and array configurations can also be specified. We leverage QuaDRiGa to provide a more realistic depolarization and antenna model with which to validate the proposed methods.

QuaDRiGa generates the continuous-time complex channel response for each transmit/receive antenna pair, which must be converted to the frequency domain unpolarized channel. To obtain the unpolarized channel, each array element consists of two co-located antennas with orthogonal polarizations. As described in Section II-B, this creates the virtual dual-polarized channel, which will be converted to the physical channel through the polarization matrices. We choose the corresponding antenna polarizations to be locally horizontal and vertical.

The effects of pulse-shaping and sampling must be incorporated into the QuaDRiGa channel output to obtain a channel matrix corresponding to (19). QuaDRiGa outputs the continuous-time channel coefficients corresponding to each path $\mathbf{H}_{up}^{(\ell)}$ and the corresponding path delays τ_{ℓ} . The bandlimited baseband channel $\mathbf{H}_{bb}(\tau)$ is obtained by convolving the channel response with the pulse-shaping filter as

$$\mathbf{H}_{\mathsf{bb}}(\tau) = \frac{1}{T}v(\tau) * \left(\sum_{\ell=1}^{L} \mathbf{H}_{\mathsf{up}}^{(\ell)} \delta(\tau - \tau_{\ell})\right)$$
(63)

$$= \sum_{\ell=1}^{L} v(\tau - \tau_{\ell}) \mathbf{H}_{\mathsf{up}}^{(\ell)}. \tag{64}$$

The frequency-domain response is obtained by sampling and taking the discrete Fourier transform,

$$\mathbf{H}_{\mathsf{up},k} = \sum_{\ell=1}^{L} \mathsf{v}_{\ell}[k] \mathbf{H}_{\mathsf{up}}^{(\ell)}. \tag{65}$$

The expressions in (13) and (65) are used to convert the QuaDRiGa outputs $\mathbf{H}_{up}^{(\ell)}$ and τ_{ℓ} to the frequency domain channel $\mathbf{H}_{up,k}$. The unpolarized channel is normalized as discussed in the prior section.

We simulate an outdoor urban microcell (UMi) deployment operating at 2.6 GHz with a bandwidth of 5 MHz. The transmitter transmits four data streams over K=256 subcarriers. As in the previous section, a raised-cosine filter with rolloff factor 0.3 is used for pulse-shaping filter. The antenna arrays are comprised of triangular bowtie antennas that are designed to operate at 2.6 GHz using the MATLABTM Antenna Toolbox. The antennas are vertically polarized and

exhibit a weak pattern in the cross-pol direction. In all of the following simulations, the transmitter and receiver are both equipped with uniform linear arrays each composed of four antennas spaced at half-wavelength. The transmitter is located at the origin at a height of 1.5 m. Denoting D_r as the distance from the origin to the receiver in meters and ξ_r as the azimuthal angle, the receiver location is randomly placed at a location $(D_r \cos \xi_r, D_r \sin \xi_r, 1.5 \, \text{m})$. We assume D_r is uniformly distributed in the range [50, 250] m and ξ_r is uniformly distributed in $[0, 2\pi)$.

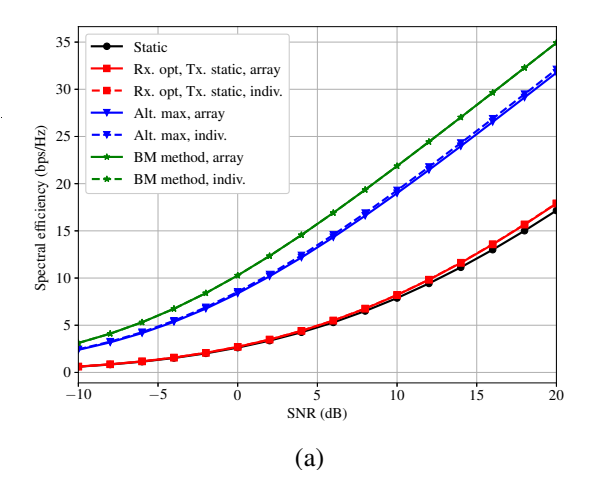
In Figs. 4, we compare the achieved spectral efficiencies of the proposed polarization optimization algorithms. As an additional baseline, we also include an alternating minimization which iteratively uses the single-sided polarization at the transmitter and the receiver. The algorithm uses a few alternating optimizations using the output of the "Rx opt., Tx static" algorithm. Results for a line-of-sight (LOS) scenario are shown in Fig. 4(a), and results for a non-LOS (NLOS) scenario with 20 paths are shown in Fig. 4(b). In both cases, the BM algorithm achieves a significant gain in spectral efficiency over the static and even alternating maximization algorithms. Comparing both scenarios, the polarization reconfiguration achieves higher gain in the LOS case because the number paths in the NLOS case prevent polarization reconfiguration from properly aligning with all of the paths. As before, the perarray optimization performs nearly-identically to the individual reconfiguration except for the alternating maximization algorithm. This is because the optimization paths in the iterative process quickly diverge for the two levels of reconfiguration.

The effect of quantization on polarization reconfiguration is shown in Fig. 5. The number of bits is assumed to be the same at both the transmitter and receiver. The BM method showcases robustness to the effects of quantization and a significant gain over the static method. By implementing the BM method with one-bit polarization quantization and the perarray method, a single bit of feedback can double the spectral efficiency compared to the static case.

VII. CONCLUSION

We have developed strategies for efficient polarization reconfiguration in a wideband MIMO system. We leveraged a double-directional channel model to show that adapting the array polarization effectively performs a pre- or post-coding operation on an unpolarized version of the channel. We derived closed-form expressions for the unilateral polarization configuration and highlighted the relationship between the optimal solution and the eigendecomposition of the unilaterally polarized channel. We also developed upper bounds on the system performance, and used these bounds to create a low-complexity method for joint polarization optimization. Simulation results demonstrate that simple polarization reconfiguration techniques, such as the subarray method and the bound maximization approach, achieve near-optimal performance in a variety of settings.

The characteristics of polarization reconfigurable communication open up a number of relevant future research directions. While we leveraged polarization reconfiguration to minimize



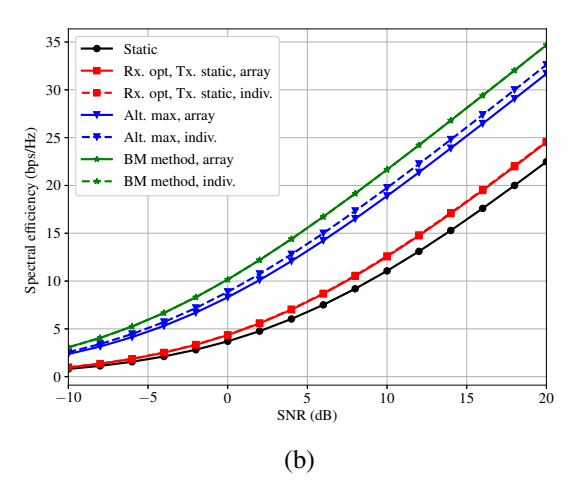


Fig. 4: Spectral efficiency vs. SNR for different polarization reconfiguration methods in a UMi wideband deployment with LOS propagation in (a) and NLOS propagation in (b). The number of paths slightly reduces the effectiveness of reconfiguration compared to the LOS scenario.

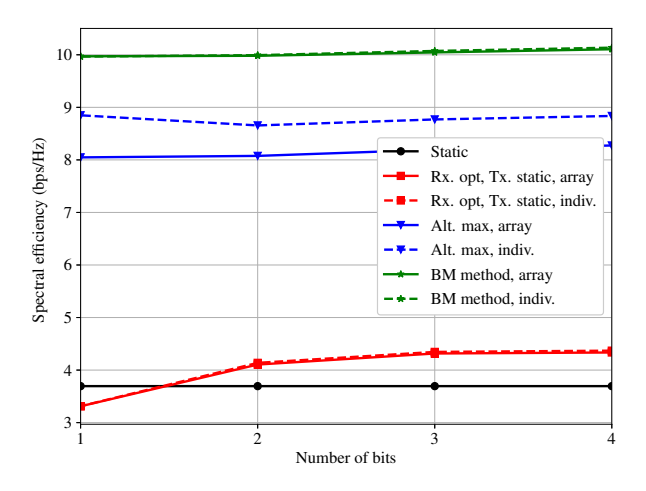


Fig. 5: Spectral efficiency vs. the number of quantization bits at SNR = 10 dB. Successful polarization reconfiguration is possible even with a single bit of overhead.

the polarization mismatch induced by the antennas and the wireless channel, this mismatch could equivalently be maximized to mitigate interference in multi-user communication. Polarization precoding codebooks can also be leveraged to provide the benefits of polarization diversity while minimizing overhead. This work also highlights the importance of estimating the unpolarized channel matrix, which accounts for wireless propagation across all possible polarizations. While prior techniques on channel estimation could be used for this purpose, polarization reconfiguration could also be used to design efficient channel estimation algorithms that take advantage of the common parameters in the channel for different polarizations. Reconfigurable arrays increase communication flexibility with a limited cost, and there are many open opportunities to study their performance in the context of MIMO.

REFERENCES

- M. R. Castellanos and R. W. Heath, "MIMO communication with polarization reconfigurable antennas," in *Proc. 55th Asilomar Conf. Signals, Syst., Comput.*, Pacific Grove, CA, USA, Nov. 2021, pp. 1– 5.
- [2] J. Costantine, Y. Tawk, S. E. Barbin, and C. G. Christodoulou, "Reconfigurable antennas: Design and applications," *Proc. IEEE*, vol. 103, no. 3, pp. 424–437, Mar. 2015.
- [3] R. L. Haupt and M. Lanagan, "Reconfigurable antennas," *IEEE Antennas Propag. Mag.*, vol. 55, no. 1, pp. 49–61, Feb. 2013.
- [4] N. Ojaroudi Parchin, H. Jahanbakhsh Basherlou, Y. I. A. Al-Yasir, R. A. Abd-Alhameed, A. M. Abdulkhaleq, and J. M. Noras, "Recent developments of reconfigurable antennas for current and future wireless communication systems," *Electron.*, vol. 8, no. 2, 2019.
- [5] M. Shirazi, J. Huang, T. Li, and X. Gong, "A switchable-frequency slot-ring antenna element for designing a reconfigurable array," *IEEE Antennas Wireless Propag. Lett.*, vol. 17, no. 2, pp. 229–233, Feb. 2018.
- [6] D. Piazza, P. Mookiah, M. D'Amico, and K. R. Dandekar, "Experimental analysis of pattern and polarization reconfigurable circular patch antennas for MIMO systems," *IEEE Trans. Veh. Technol.*, vol. 59, no. 5, pp. 2352–2362, Jun. 2010.
- [7] A. M. Sayeed and V. Raghavan, "Maximizing MIMO capacity in sparse multipath with reconfigurable antenna arrays," *IEEE J. Sel. Areas Commun.*, vol. 1, no. 1, pp. 156–166, Jun. 2007.
- [8] H. Do, N. Lee, and A. Lozano, "Reconfigurable ULAs for line-of-sight MIMO transmission," *IEEE Trans. Wireless Commun.*, vol. 20, no. 5, pp. 2933–2947, May 2021.
- [9] Y. P. Selvam, L. Elumalai, M. G. N. Alsath, M. Kanagasabai, S. Subbaraj, and S. Kingsly, "Novel frequency- and pattern-reconfigurable rhombic patch antenna with switchable polarization," *IEEE Antennas Wireless Propag. Lett.*, vol. 16, pp. 1639–1642, 2017.
- [10] B. A. Cetiner, G. Roqueta Crusats, L. Jofre, and N. Biyikli, "RF MEMS integrated frequency reconfigurable annular slot antenna," *IEEE Trans. Antennas Propag.*, vol. 58, no. 3, pp. 626–632, 2010.
- [11] D. Anagnostou, G. Zheng, M. Chryssomallis, J. Lyke, G. Ponchak, J. Papapolymerou, and C. Christodoulou, "Design, fabrication, and measurements of an RF-MEMS-based self-similar reconfigurable antenna," *IEEE Trans. Antennas Propag.*, vol. 54, no. 2, pp. 422–432, 2006.
- [12] Y. I. A. Al-Yasir, A. S. Abdullah, N. Ojaroudi Parchin, R. A. Abd-Alhameed, and J. M. Noras, "A new polarization-reconfigurable antenna for 5G applications," *Electron.*, vol. 7, no. 11, 2018.
- [13] S.-A. Malakooti and C. Fumeaux, "Pattern-reconfigurable antenna with switchable wideband to frequency-agile bandpass/bandstop filtering operation," *IEEE Access*, vol. 7, pp. 167 065–167 075, 2019.
- [14] P. K. Li, Z. H. Shao, Q. Wang, and Y. J. Cheng, "Frequency- and patternreconfigurable antenna for multistandard wireless applications," *IEEE Antennas Wireless Propag. Lett.*, vol. 14, pp. 333–336, 2015.
- [15] A. Mansoul, F. Ghanem, M. R. Hamid, E. Salonen, and M. Berg, "Bandwidth reconfigurable antenna with a fixed lower and a variable upper limit," *IET Microw., Antennas, Propag.*, vol. 10, no. 15, pp. 1725– 1733, 2016.
- [16] I. T. Nassar, H. Tsang, D. Bardroff, C. P. Lusk, and T. M. Weller, "Mechanically reconfigurable, dual-band slot dipole antennas," *IEEE Trans. Antennas Propag.*, vol. 63, no. 7, pp. 3267–3271, 2015.

- [17] J. Costantine, Y. Tawk, J. Woodland, N. Flaum, and C. G. Christodoulou, "Reconfigurable antenna system with a movable ground plane for cognitive radio," *IET Microw., Antennas, Propag.*, vol. 8, no. 11, pp. 858–863, 2014.
- [18] T. Li and Z. N. Chen, "A dual-band metasurface antenna using characteristic mode analysis," *IEEE Trans. Antennas Propag.*, vol. 66, no. 10, pp. 5620–5624, 2018.
- [19] S. S. Syed Nasser, W. Liu, and Z. N. Chen, "Wide bandwidth and enhanced gain of a low-profile dipole antenna achieved by integrated suspended metasurface," *IEEE Trans. Antennas Propag.*, vol. 66, no. 3, pp. 1540–1544, 2018.
- [20] N. Hussain and I. Park, "Design of a wide-gain-bandwidth metasurface antenna at terahertz frequency," AIP Advances, vol. 7, no. 5, p. 055313, 2017.
- [21] S. X. Ta and I. Park, "Compact wideband circularly polarized patch antenna array using metasurface," *IEEE Antennas Wireless Propag. Lett.*, vol. 16, pp. 1932–1936, 2017.
- [22] T. Li and Z. N. Chen, "Wideband substrate-integrated waveguide-fed endfire metasurface antenna array," *IEEE Trans. Antennas Propag.*, vol. 66, no. 12, pp. 7032–7040, 2018.
- [23] N.-S. Nie, X.-S. Yang, Z. N. Chen, and B.-Z. Wang, "A low-profile wideband hybrid metasurface antenna array for 5G and WiFi systems," *IEEE Trans. Antennas Propag.*, vol. 68, no. 2, pp. 665–671, 2020.
- [24] W. Yang, S. Chen, W. Che, Q. Xue, and Q. Meng, "Compact high-gain metasurface antenna arrays based on higher-mode SIW cavities," *IEEE Trans. Antennas Propag.*, vol. 66, no. 9, pp. 4918–4923, 2018.
- [25] J. Hu, G. Q. Luo, and Z.-C. Hao, "A wideband quad-polarization reconfigurable metasurface antenna," *IEEE Access*, vol. 6, pp. 6130– 6137, Oct. 2018.
- [26] K. Y. Alqurashi, J. R. Kelly, Z. Wang, C. Crean, R. Mittra, M. Khalily, and Y. Gao, "Liquid metal bandwidth-reconfigurable antenna," *IEEE Antennas and Wireless Propag. Lett.*, vol. 19, no. 1, pp. 218–222, Jan. 2020.
- [27] V. T. Bharambe, J. Ma, M. D. Dickey, and J. J. Adams, "RESHAPE: A liquid metal-based reshapable aperture for compound frequency, pattern, and polarization reconfiguration," *IEEE Trans. Antennas Propag.*, vol. 69, no. 5, pp. 2581–2594, May 2021.
- [28] Z. Chen, H. Wong, and J. Kelly, "A polarization-reconfigurable glass dielectric resonator antenna using liquid metal," *IEEE Trans. Antennas Propag.*, vol. 67, no. 5, pp. 3427–3432, May 2019.
- [29] D. Rodrigo, L. Jofre, and B. A. Cetiner, "Circular beam-steering reconfigurable antenna with liquid metal parasitics," *IEEE Trans. Antennas Propag.*, vol. 60, no. 4, pp. 1796–1802, Apr. 2012.
- [30] J. D. Boerman and J. T. Bernhard, "Performance study of pattern reconfigurable antennas in MIMO communication systems," *IEEE Trans. Antennas Propag.*, vol. 56, no. 1, pp. 231–236, Jan. 2008.
- [31] T. Zhao, M. Li, and Y. Pan, "Online learning based reconfigurable antenna mode selection exploiting channel correlation," *IEEE Trans. Wireless Commun.*, vol. 20, no. 10, pp. 6820–6834, Oct. 2021.
- [32] M. Hasan, İ. Bahçeci, and B. A. Cetiner, "Downlink multi-user MIMO transmission for radiation pattern reconfigurable antenna systems," *IEEE Trans. Wireless Commun.*, vol. 17, no. 10, pp. 6448–6463, Oct. 2018.
- [33] Y. Hou, M. Li, and K. Zeng, "Throughput optimization in multi-hop wireless networks with reconfigurable antennas," in *Proc. Int. Conf. Comput.*, Netw. Commun. (ICNC), Jan. 2017, pp. 620–626.
- [34] H. Eslami, C. P. Sukumar, D. Rodrigo, S. Mopidevi, A. M. Eltawil, L. Jofre, and B. A. Cetiner, "Reduced overhead training for multi reconfigurable antennas with beam-tilting capability," *IEEE Trans. Wireless Commun.*, vol. 9, no. 12, pp. 3810–3821, Dec. 2010.
- [35] S.-C. Kwon and A. F. Molisch, "Capacity maximization with polarization-agile antennas in the MIMO communication system," in *Proc. IEEE Global Commun. Conf. (GLOBECOM)*, San Diego, CA, USA, Feb. 2015, pp. 1–6.
- [36] S. H. Doan, S.-C. Kwon, and H.-G. Yeh, "Achievable capacity of multipolarization MIMO with the practical polarization-agile antennas," *IEEE Syst. J.*, pp. 1–12, Jun. 2020.
- [37] J. Huang, M. Shirazi, and X. Gong, "A new arraying technique for band-switchable and polarization-reconfigurable antenna arrays with wide bandwidth," *IEEE Open J. Antennas Propag.*, vol. 3, pp. 1025–1040, 2022.
- [38] N. Shlezinger, G. C. Alexandropoulos, M. F. Imani, Y. C. Eldar, and D. R. Smith, "Dynamic metasurface antennas for 6G extreme massive MIMO communications communications," *IEEE Wireless Commun.*, vol. 28, no. 2, pp. 106–113, Apr. 2021.
- [39] T. Kim, B. Clerckx, D. J. Love, and S. J. Kim, "Limited feedback beamforming systems for dual-polarized MIMO channels," *IEEE Trans. Wireless Commun.*, vol. 9, no. 11, pp. 3425–3439, Nov. 2010.

- [40] J. Park and B. Clerckx, "Multi-user linear precoding for multi-polarized massive MIMO system under imperfect CSIT," *IEEE Trans. on Wireless Commun.*, vol. 14, no. 5, pp. 2532–2547, May 2015.
- [41] G. Zafari, M. Koca, and H. Sari, "Dual-polarized spatial modulation over correlated fading channels," *IEEE Trans. Commun.*, vol. 65, no. 3, pp. 1336–1352, Mar. 2017.
- [42] J. Zhang, K. J. Kim, A. A. Glazunov, Y. Wang, L. Ding, and J. Zhang, "Generalized polarization-space modulation," *IEEE Trans. Commun.*, vol. 68, no. 1, pp. 258–273, Jan. 2020.
- [43] D. Zhu, J. Choi, and R. W. Heath, "Two-dimensional AoD and AoA acquisition for wideband millimeter-wave systems with dual-polarized MIMO," *IEEE Trans. Wireless Commun.*, vol. 16, no. 12, pp. 7890–7905, Dec. 2017.
- [44] C. Qian, X. Fu, N. D. Sidiropoulos, and Y. Yang, "Tensor-based channel estimation for dual-polarized massive MIMO systems," *IEEE Trans. Signal. Process.*, vol. 66, no. 24, pp. 6390–6403, Dec. 2018.
- [45] J. Song, J. Choi, S. G. Larew, D. J. Love, T. A. Thomas, and A. A. Ghosh, "Adaptive millimeter wave beam alignment for dual-polarized MIMO systems," *IEEE Trans. Wireless Commun.*, vol. 14, no. 11, pp. 6283–6296, Nov. 2015.
- [46] L. A. Gutierrez, S. An, S. S.-C. Kwon, and H.-G. Yeh, "Novel approach of spatial modulation: Polarization-aware OFDM subcarrier allocation," in *Proc. IEEE Green Energy Smart Sys. Conf. (IGESSC)*, 2020, pp. 1–6.
- [47] Y. Wang, D. Piao, and J. Song, "Implementation and MIMO performance assessment of two quad-polarized antennas," *IEEE Antennas Wireless Propag. Lett.*, vol. 21, no. 12, pp. 2332–2336, Dec. 2022.
- [48] P. Oh and S. Kwon, "Multi-polarization superposition beamforming with XPD-aware transmit power allocation," in *Proc. IEEE 92nd Veh. Technol. Conf. (VTC-Fall)*, Victoria, BC, Canada, Nov. 2020, pp. 1–6.
- [49] R. Bhagavatula, C. Oestges, and R. W. Heath, "A new double-directional channel model including antenna patterns, array orientation, and depolarization," *IEEE Trans. Veh. Technol.*, vol. 59, no. 5, pp. 2219–2231, Jun. 2010.
- [50] S. Park, A. Alkhateeb, and R. W. Heath, "Dynamic subarrays for hybrid precoding in wideband mmWave MIMO systems," *IEEE Trans. Wireless Commun.*, vol. 16, no. 5, pp. 2907–2920, May 2017.
- [51] H. Sarieddeen, M. Alouini, and T. Y. Al-Naffouri, "Terahertz-band ultra-massive spatial modulation MIMO," *IEEE J. Sel. Areas Commun.*, vol. 37, no. 9, pp. 2040–2052, Sep. 2019.
- [52] A. A. Nasir, S. Durrani, H. Mehrpouyan, S. D. Blostein, and R. A. Kennedy, "Timing and carrier synchronization in wireless communication systems: a survey and classification of research in the last 5 years," *EURASIP J. Wireless Commun. Netw.*, vol. 2016, pp. 1–38, 2016.
- [53] R. W. Heath and A. Lozano, Foundations of MIMO Communications. Cambridge University Press, 2018.
- [54] M. J. Kronenburg, "A method for fast diagonalization of a 2x2 or 3x3 real symmetric matrix," 2013. [Online]. Available: https://arxiv.org/abs/1306.6291
- [55] C. C. Paige and M. Wei, "History and generality of the CS decomposition," *Linear Algebra Appl.*, vol. 208, pp. 303–326, 1994.
- [56] W. Fulton, "Eigenvalues of sums of Hermitian matrices," Séminaire Bourbaki, vol. 40, pp. 255–269, 1998.
- [57] R. A. Horn and C. R. Johnson, *Matrix analysis*. Cambridge, U.K.: Cambridge Univ. Press, 2012.
- [58] V. Raghavan, J. Cezanne, S. Subramanian, A. Sampath, and O. Koymen, "Beamforming tradeoffs for initial UE discovery in millimeter-wave MIMO systems," *IEEE J. Sel. Topics Signal Process.*, vol. 10, no. 3, pp. 543–559, Jan. 2016.
- [59] S. Jaeckel, L. Raschkowski, K. Börner, and L. Thiele, "QuaDRiGa: A 3-D multi-cell channel model with time evolution for enabling virtual field trials," *IEEE Transactions on Antennas and Propagation*, vol. 62, no. 6, pp. 3242–3256, June 2014.



Miguel R. Castellanos (S'18 - M'20) received the B.S. degree (with highest distinction) and Ph.D in electrical engineering from Purdue University, West Lafayette, IN, USA, in 2015 and 2020, respectively. He is currently a postdoctoral researcher and has been with The University of Texas at Austin (2020-2021) and North Carolina State University (2021-present). During the summers of 2017 and 2019, he was a research intern at Qualcomm Flarion Technologies, Bridgewater, NJ, USA and at Nokia Networks, Naperville, IL, USA, respectively. His

research interests include massive MIMO, near-field communication, antenna theory, exposure-constrained communication, and signal processing. He co-authored a paper that won the 2022 Fred W. Ellersick MILCOM Best Paper Award and the 2022 Vanu Bose Best Paper Award.



Robert W. Heath Jr. (S'96 - M'01 - SM'06 - F'11) received the B.S. and M.S. degrees from the University of Virginia, Charlottesville, VA, in 1996 and 1997 respectively, and the Ph.D. from Stanford University, Stanford, CA, in 2002, all in electrical engineering. From 1998 to 2001, he was a Senior Member of the Technical Staff then a Senior Consultant at Iospan Wireless Inc, San Jose, CA where he worked on the design and implementation of the physical and link layers of the first commercial MIMO-OFDM communication system. From 2002-

2020 he was with The University of Texas at Austin, most recently as Cockrell Family Regents Chair in Engineering and Director of UT SAVES. He is presently the Lampe Distinguished Professor at North Carolina State University and co-founder of 6GNC. He is also President and CEO of MIMO Wireless Inc. He authored "Introduction to Wireless Digital Communication" (Prentice Hall, 2017) and "Digital Wireless Communication: Physical Layer Exploration Lab Using the NI USRP" (National Technology and Science Press, 2012), and co-authored "Millimeter Wave Wireless Communications" (Prentice Hall, 2014) and "Foundations of MIMO Communication" (Cambridge University Press, 2018).

Dr. Heath has been a co-author of a number award winning conference and journal papers including recently the 2017 Marconi Prize Paper Award, the 2019 IEEE Communications Society Stephen O. Rice Prize, the 2020 IEEE Signal Processing Society Donald G. Fink Overview Paper Award, the 2021 IEEE Vehicular Technology Society Neal Shepherd Memorial Best Propagation Paper Award, and the 2022 IEEE Vehicular Technology Society Best Vehicular Electronics Paper Award. Other notable awards include the 2017 EURASIP Technical Achievement award, the 2019 IEEE Kiyo Tomiyasu Award and the 2021 IEEE Vehicular Technology Society James Evans Avant Garde Award. In 2017, he was selected as a Fellow of the National Academy of Inventors. He is a member-at-large on the IEEE Communications Society Board-of-Governors (2020-2022) and is a past member-at-large on the IEEE Signal Processing Society Board-of-Governors (2016-2018). He was Editorin-Chief of IEEE Signal Processing Magazine from 2018-2020. He is also a licensed Amateur Radio Operator, a Private Pilot, a registered Professional Engineer in Texas.